Quantum Sensing of Magnetic and Thermal Fields Using Nitrogen-Vacancy Centers on Spoof Surface Plasmon Waveguides

MAXWELL STONHAM

THESIS DEFENSE

NV Centers in Fluorescent Nanodiamonds

- Crystal defects in diamonds introduce an impurity, the nitrogen-vacancy (NV) center within its carbon lattice.
- Formed by a nitrogen atom and a vacancy (missing carbon atom) within the adjacent lattice and are 35 – 100 nm small.
- Unique quantum behavior at room temperature.
- Magnetic with fluorescence and is coupled to the spin state (fluorescence intensity can be modulated by magnetic fields).

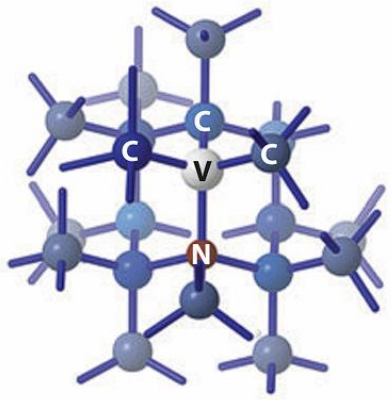

NV Centers: Optically Detected Magnetic Resonance

- Fluorescence is the light emitted by an atom or molecule due to material absorption of electromagnetic energy, occurring within nanoseconds.
- High resolution magnetic field sensing and imaging using nanodiamonds can be done by optically detected magnetic resonance (ODMR).
- Shining a green laser (532 nm) onto FND samples can excite the NV centers from the ground state to the excited state.
- After excitation, the NV centers emit red fluorescence (around 638 – 800 nm) before returning to the ground state.

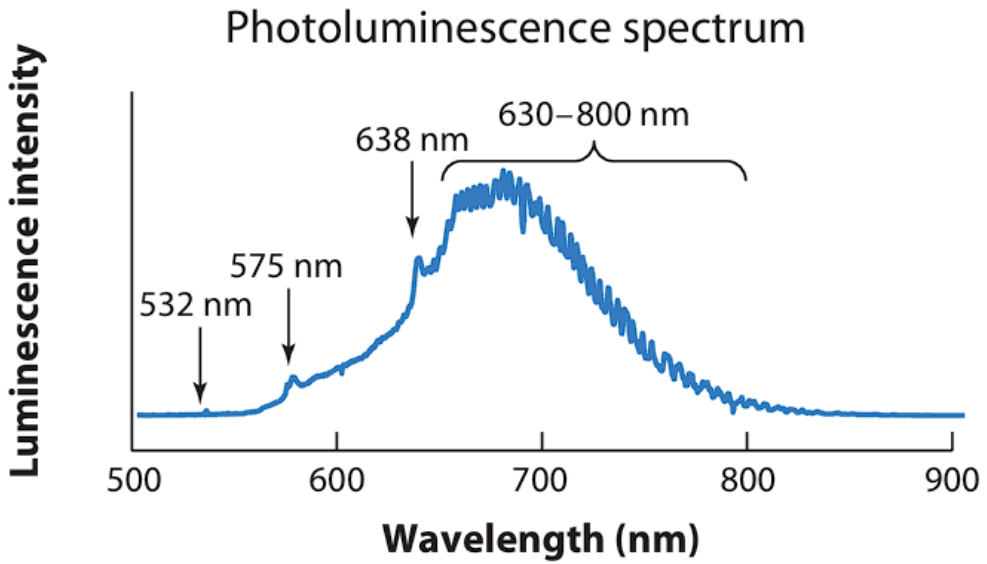

NV Centers: Energy-Level Structure

- No optical excitation: NV centers remain in the ground triplet state.
- Optical excitation: NV centers are excited to the excited state,
- After: relaxes to the ground state radiatively after 13 – 25 ns. This relaxation emits red photons.
- Non-radiative decay: through metastable state, no fluorescence since energy is lost as vibration or heat (~250ns).
- Fluorescence intensity is spin-dependent:
  - Modulated by applying a microwave signal
  - Induce transitions between spin sublevels of the ground state from ms = 0 to ms = +- 1
  - Reduction in the fluorescence.

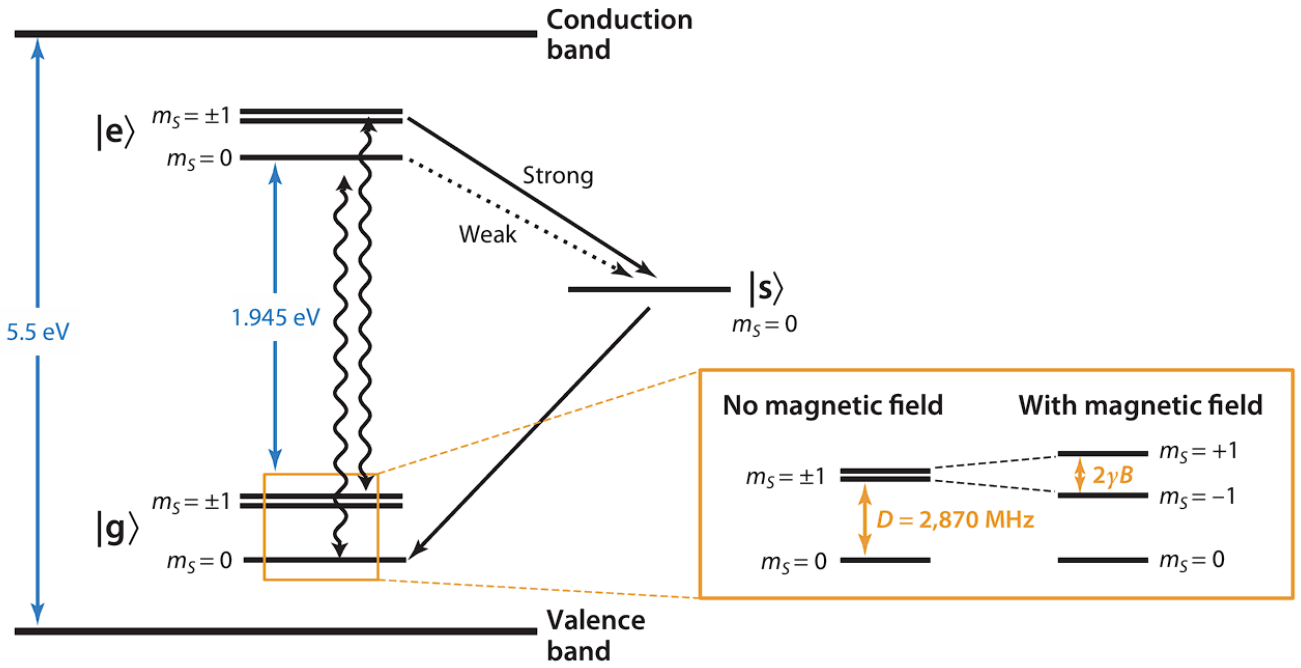

NV Centers: Quantum Sensing

- By sweeping the microwave frequency, we should be able to monitor the red fluorescence to see a dip in fluorescence (~2.87 GHz in room temperature).
- These dips correspond to the magnetic resonance conditions and are the ODMR peaks.
- The position and shape of the dips can tell us multiple things:
  - Magnetic fields: splitting of the resonance lines through the Zeeman effect
  - Temperature changes: shift in resonance frequency by -74kHz/K
  - Other parameters: electric field, strain, orientation

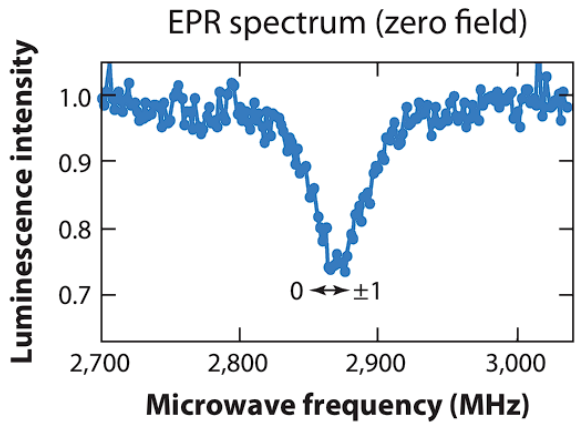

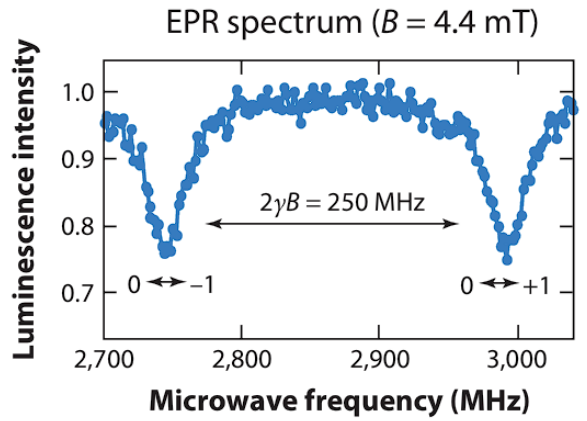

NV Centers: Quantum Sensing

Applications, Uses, and Importance

- Room-temperature quantum sensor and is highly sensitive to magnetic fields (no cryogenic cooling required).
- Biocompatible, non-toxic, and chemically inert
  - Suitable for in vivo biomedical applications such as cellular imaging, drug delivery, tissue sensing
  - Other quantum materials (cold atoms, superconductors) are incompatible within biological environments
- Uses in physics or material science: provide nanoscale-resolution maps of magnetic fields near spintronic devices or superconductors.
- Uses in biomedical: conventional fluorescent biomarkers and sensors to local environments.
- Advances in materials processing and nanoscale fabrication make it easier to create high-quality nanodiamonds with NV centers.

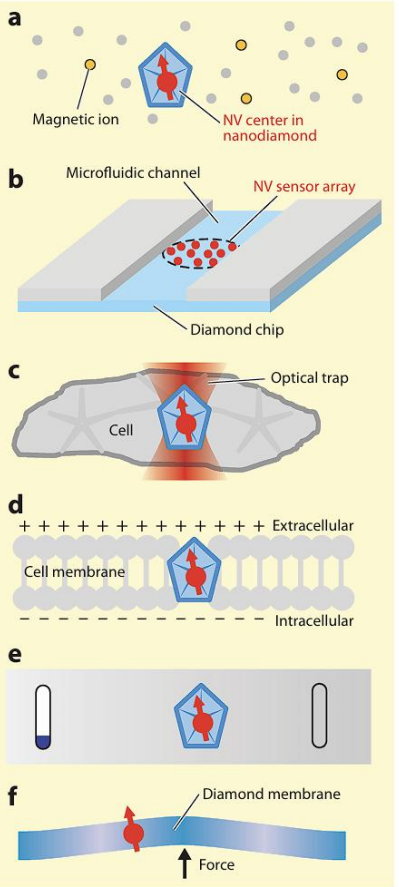

NV Centers: Quantum Sensing
Limitations

- Low photon collection efficiency:
  - Refractive index mismatch between the nanodiamond and the surrounding medium
  - Leads to light scattering
  - Lowers the number of emitted photons lowering the signal-to-noise ratio
- Charge instability between NV- to NV0:
  - Triggered by illumination, electric fields or proximity to metal surfaces
  - Can lead to unstable fluorescence
- Reduced coherence time:
  - Measure of how long a quantum state remains undisturbed/stable
  - Caused by surface defects, paramagnetic impurities, or charge noise from the surrounding environment

Overview – Spoof Surface Plasmon Polaritons

- Plasmons: Oscillations of free electrons in a metal interacting with light.
- Surface Plasmon Polaritons (SPPs): Tightly bound waves travelling along a metal-dielectric surface at optical frequencies.
- This field is evanescent (decays quickly away from the surface) which enable extreme field confinement and enhancement, making them valuable for sensing and photonic circuits.
- Issue: Metals behave like perfect conductors at microwave/THz frequencies due to negligible skin depth, producing no natural SPPs.
- Spoof SPPs: Artificially structured metal surfaces (grooves or holes) that mimic SPP behavior at low frequencies (microwave/THz).
  - These create surface-bound, evanescent fields which lead to high confinement along the metal-dielectric interface.

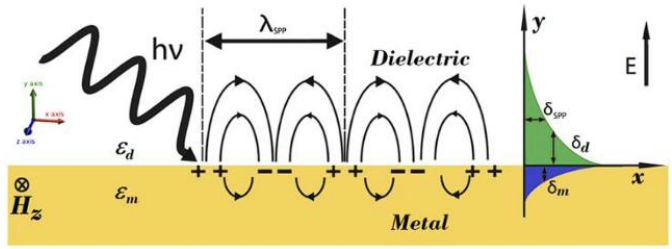

Surface plasmon polariton (SPP) showing evanescent field decay into metal and dielectric.

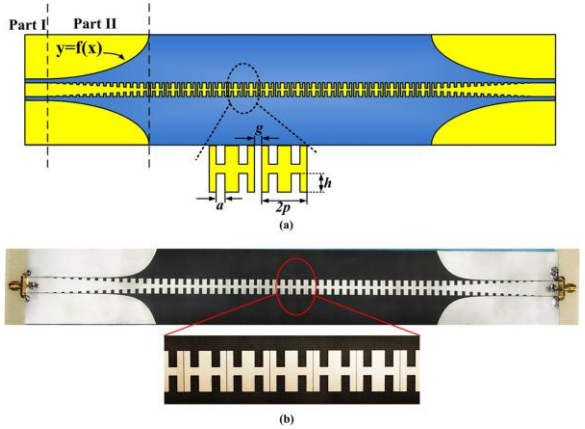

Example fabricated spoof SPP waveguide structure with periodic loading for slow-light propagation.

Motivation and why this matters?

- NV centers require localized microwave magnetic fields for efficient spin manipulation and high ODMR contrast.
- Conventional microstrips produce broad, weak field distributions that decay slowly and limits coupling efficiency (quasi-TEM modes).
- Spoof surface plasmon waveguides (SSPWs) can generate surface-bound, evanescent microwave fields that are tightly confined near the metal surface which enhances field confinement and produces stronger B-fields for spin driving (plasmonic modes).
- Integrating NV-based quantum sensors with SSPWs can increase microwave field confinement near the diamond surface, improving ODMR signal contrast, and enable efficient spin driving at lower input power.

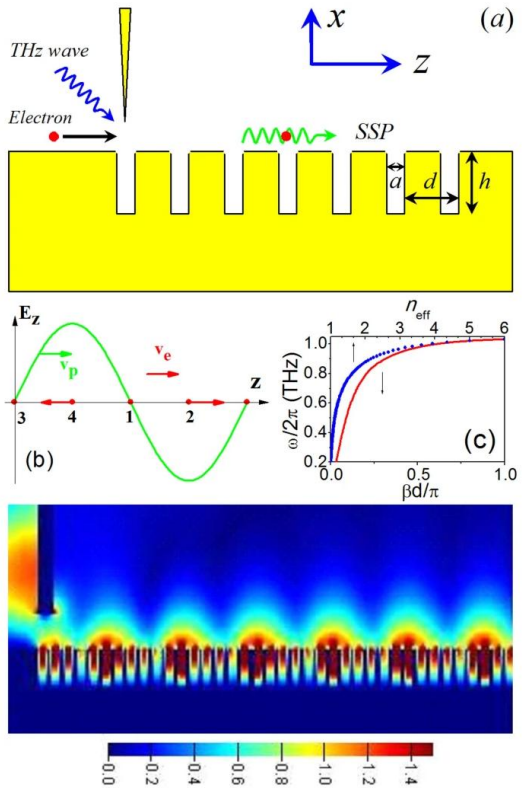

Schematic showing how SSPs can interact with free electrons, enabling acceleration or deceleration depending on phase alignment.

Theory – Planar Surfaces, 1D Grooves, 2D Dimples

- Planar metallic surfaces with periodic structures such as 1D grooves or 2D dimples were the earliest platforms used to demonstrate spoof surface plasmon behavior.
- These configurations support surface-bound plasmonic EM modes by allowing field penetration into the subwavelength features.
- Subwavelength grooves emulate a finite skin depth, letting the field penetrate into the metal and store energy similar to how optical SPPs form at finite-depth surfaces.
- By adjusting geometric parameters like groove depth, width, and periodicity, it is possible to finely tune the dispersion relation and field confinement and offer insight into how surface structuring governs plasmonic behavior.

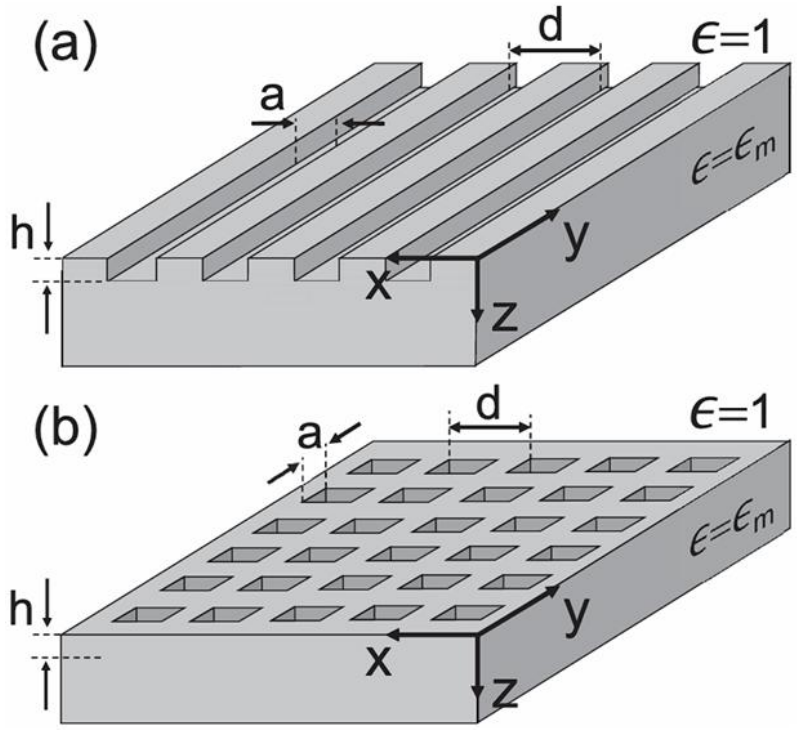

1D and 2D periodic geometries used to mimic surface plasmon behavior at low frequencies.

Prior Work: Spoof Plasmon Waveguide Design

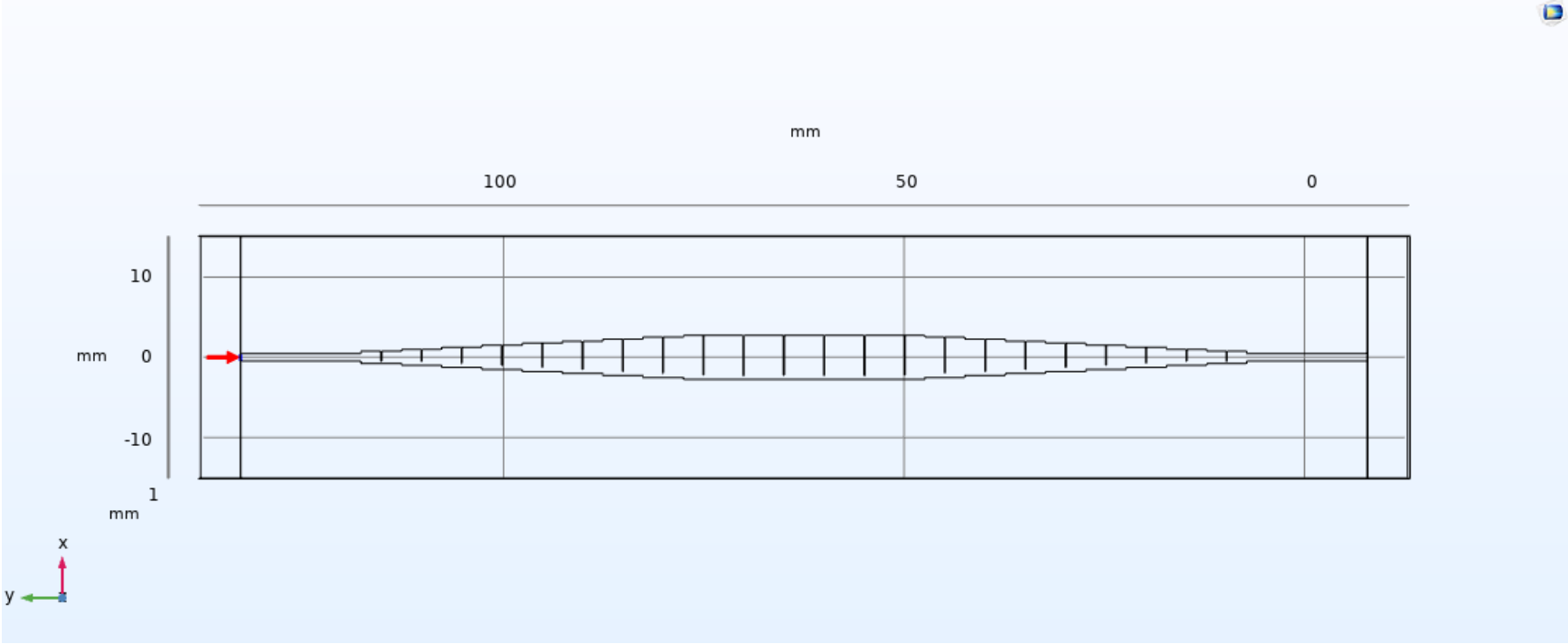

Geometry of the spoof plasmon waveguide used in the prior work by Shugayev et al. The structure consist of a planar metallic surface with periodic rectangular grooves that gradually vary in width and taper along the propagation direction to support spoof plasmon modes.

Prior Work: Gap Reduction and Field Enhancement

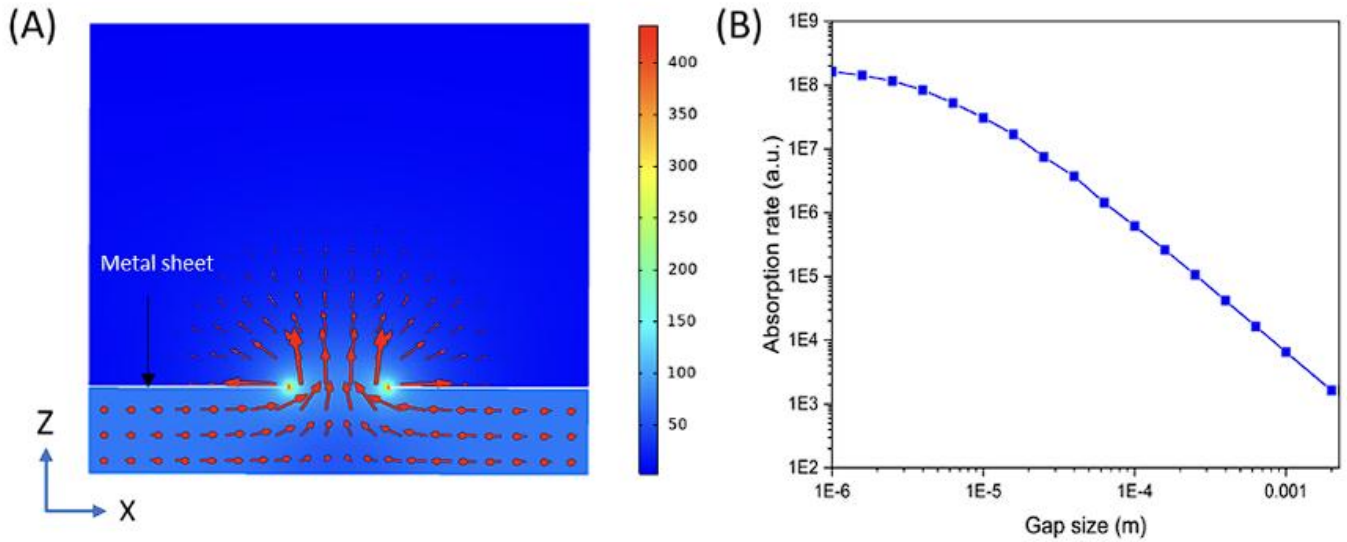

Spoof plasmon field enhancement and collection efficiency, reproduced from Shugayev et al. (A) Simulated magnetic field distribution in a unit cell of the spoof plasmon waveguide showing strong field confinement near the grooves. (B) Modeled dependence of absorption rate on gap size, illustrating enhanced field localization for narrower gaps.

Goal of this thesis:

- Experimental verification of theory:
  - Reducing gap sizes increases field enhancement
- NV center integration and ODMR characterization:
  - Magnetic field splitting
    - Observe Zeeman splitting and confirm consistency among repeated tests
  - Temperature shifting
    - Observe trends on how resonant frequencies shift and other known effects
  - Microwave power and optical power effects
    - Analyze how varying microwave power and laser intensities affect ODMR contrast, line-width and spin-driving efficiency

Initial Simulations

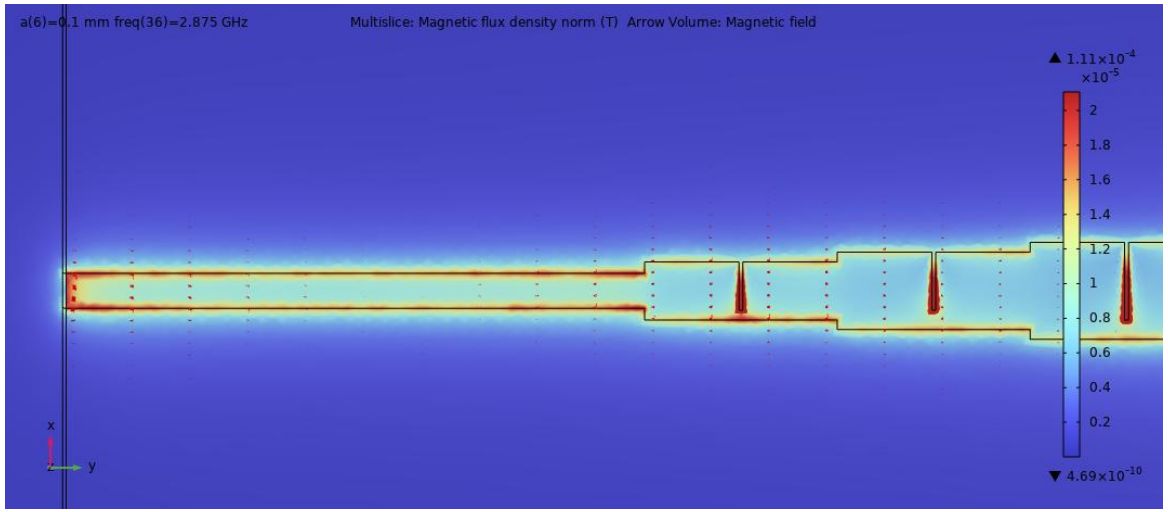

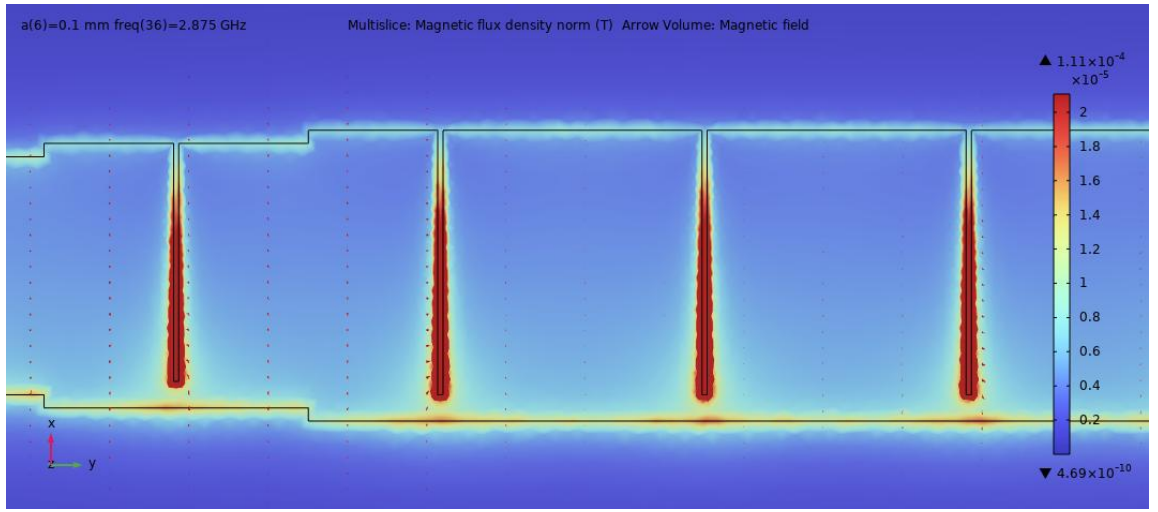

Simulated magnetic flux density distribution of the waveguide design at 2.875GHz for a periodic gap of a = 0.1mm. The color map represents the magnitude of the magnetic flux density. Strong field confinement and enhancement can be observed along the corrugated surface regions of the waveguide and indicates subwavelength mode localization.

Fabrication Process: Substrate Used

Substrate: Rogers 6010 Laminate

- Ceramic-PTFE composite
- High permittivity increases surface-mode localization (ε = 10.2)
- Low-loss tangent for lower signal attenuation (δ tan = 0.0023)
- Electrodeposited copper layer on both sides (17.5µm)
- Optimized for microwave and mm-Wave applications

Fabrication Process: Spin Coating

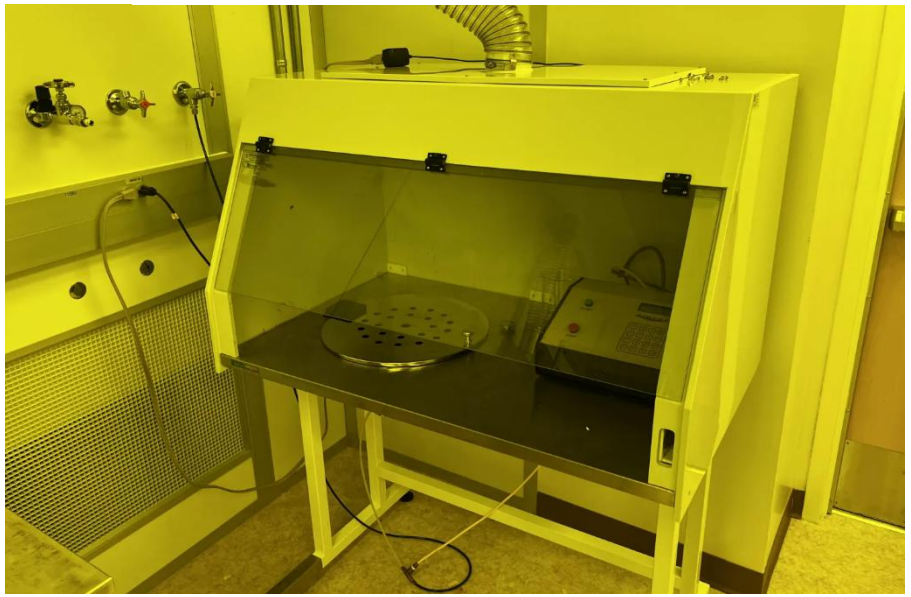

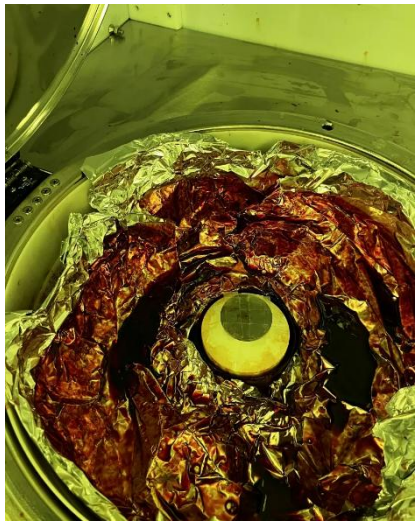

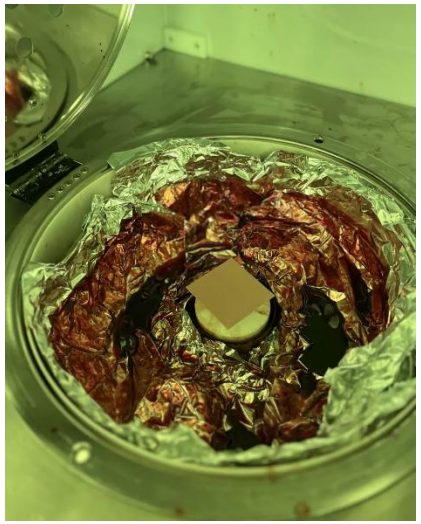

Fabrication Process: Maskless Lithography

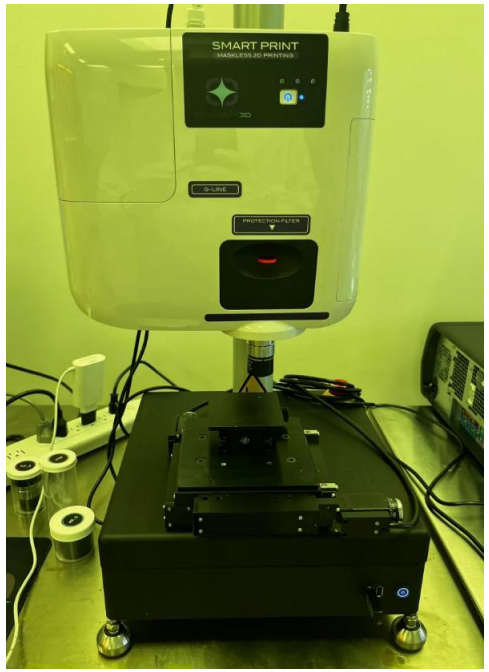

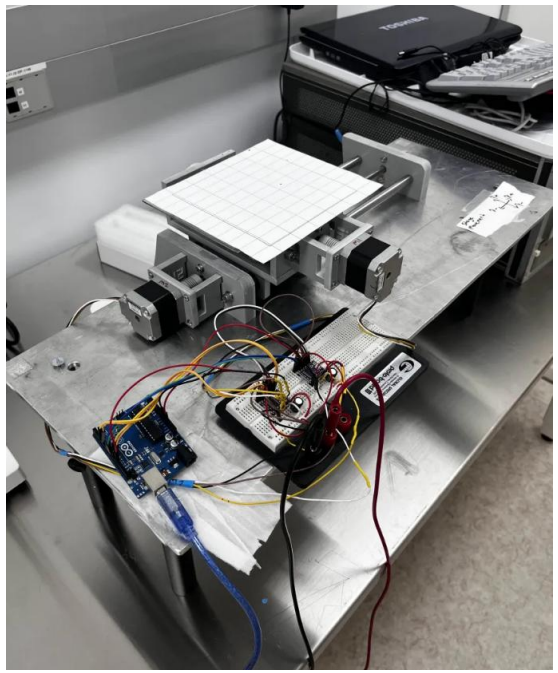

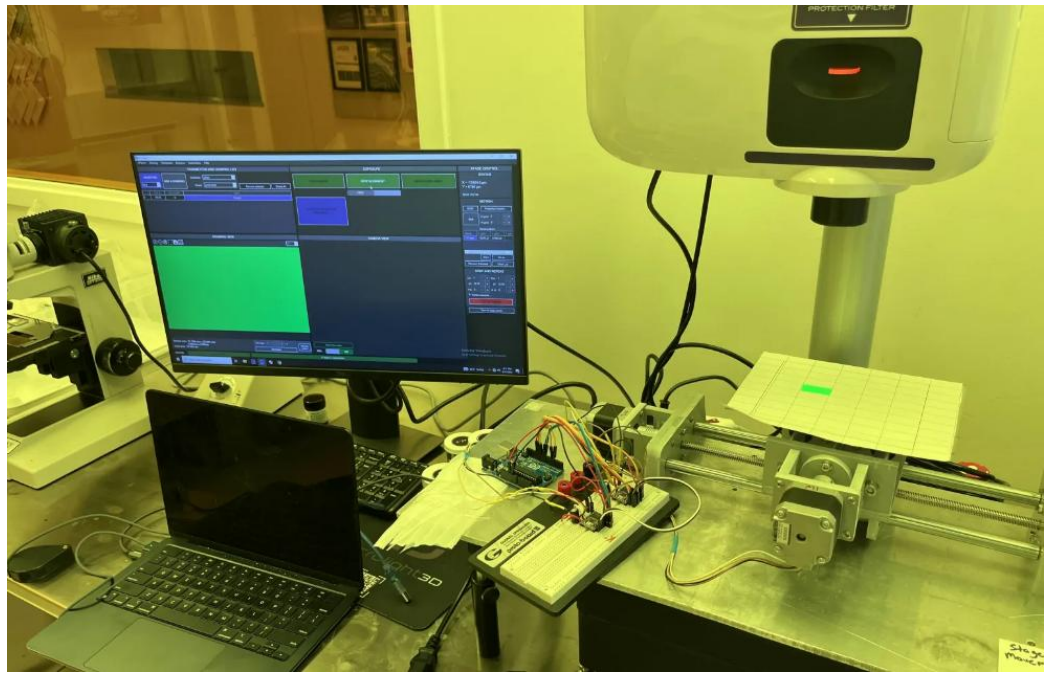

Fabrication Process: Copper Etching

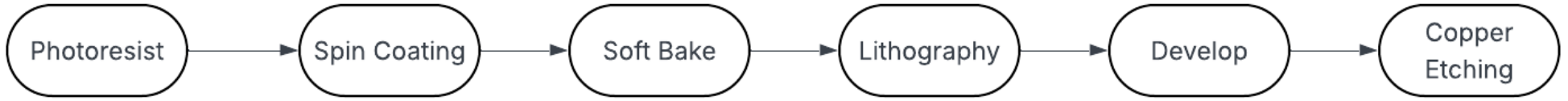

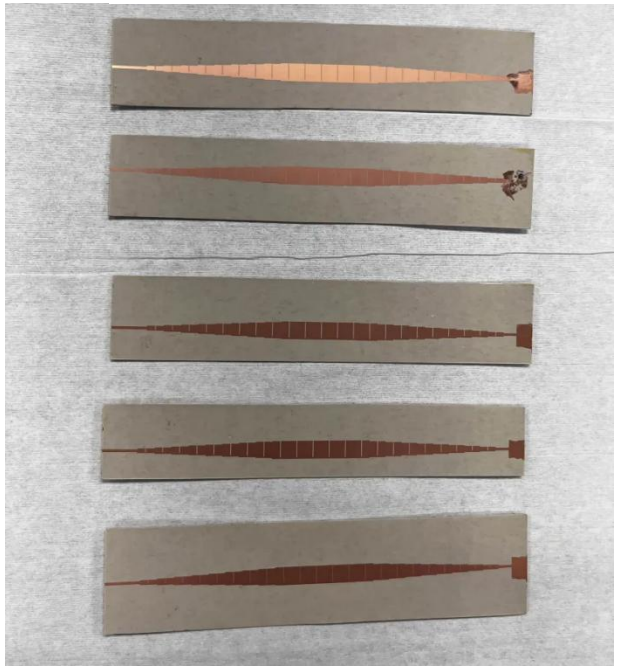

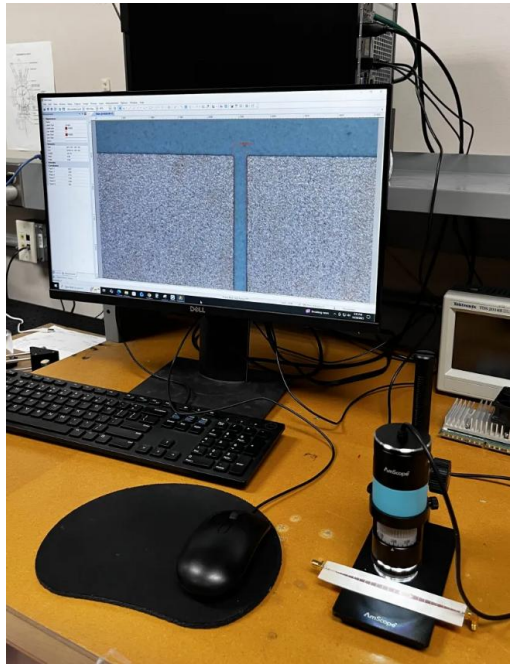

Expected Gap Size (µm)	Fabricated Gap Size (µm)	Error (µm)
40	120	80
80	145	65
120	210	90
160	275	115
200	285	85

Fabrication Process: Measurements

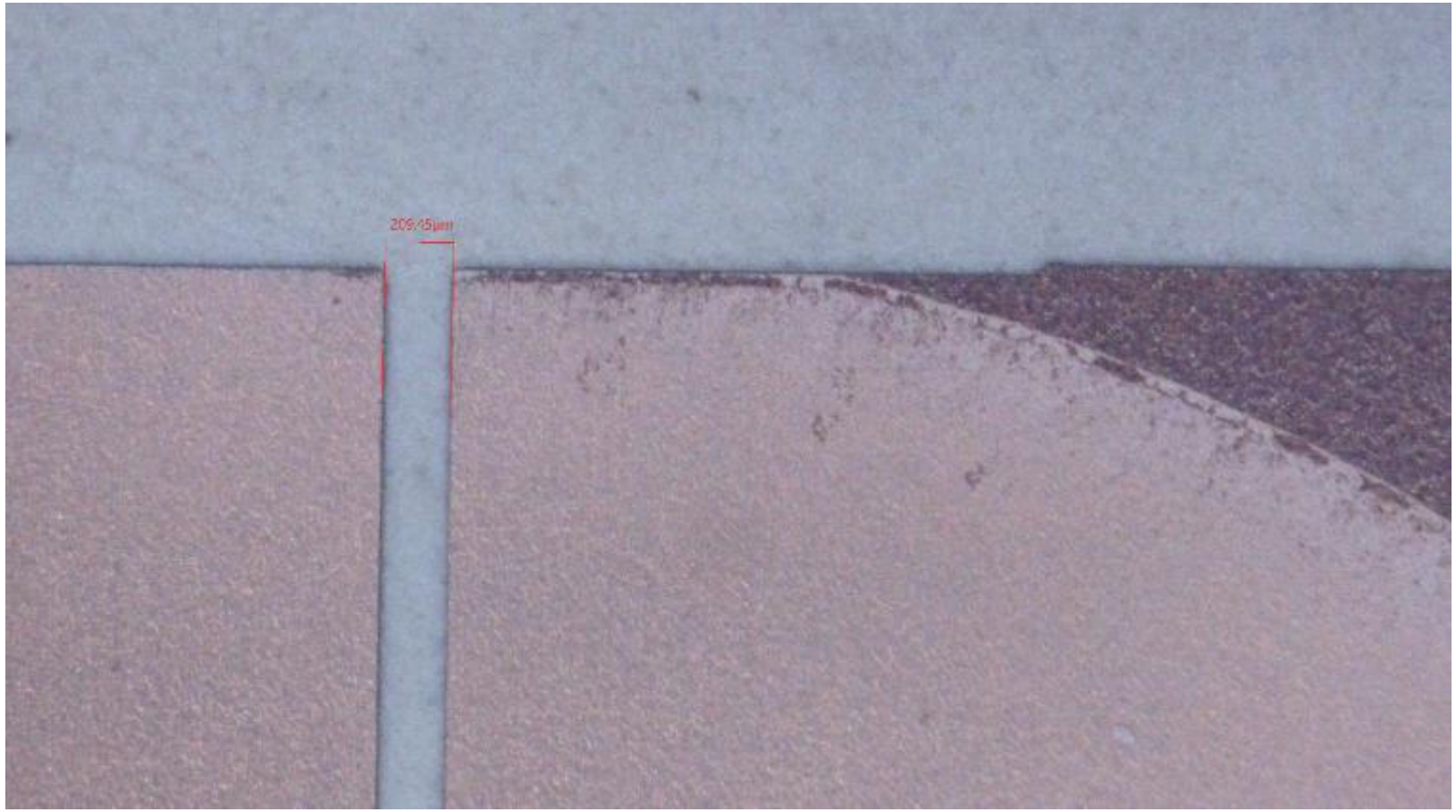

Fabrication Process: Completed Waveguides

Fabricated Designs Used

Expected Gap Size (µm)	Fabricated Gap Size (µm)	Error (µm)
40	120	80
120	210	90
200	285	85

Optical Setup

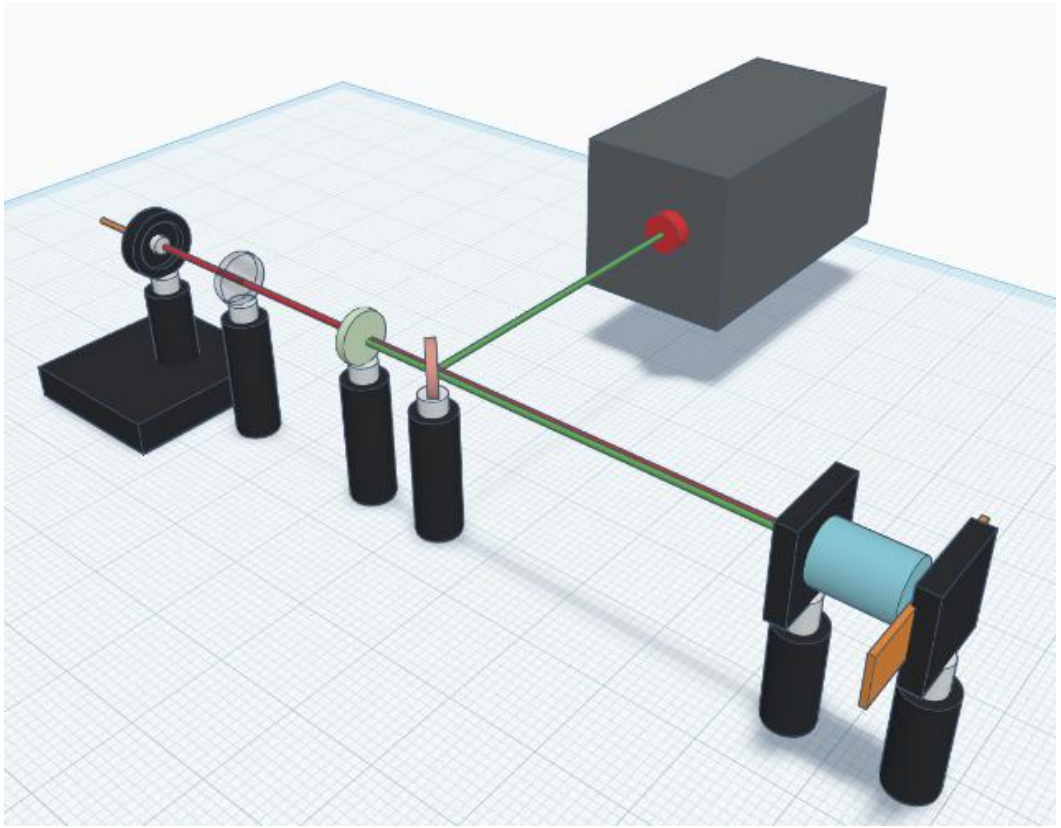

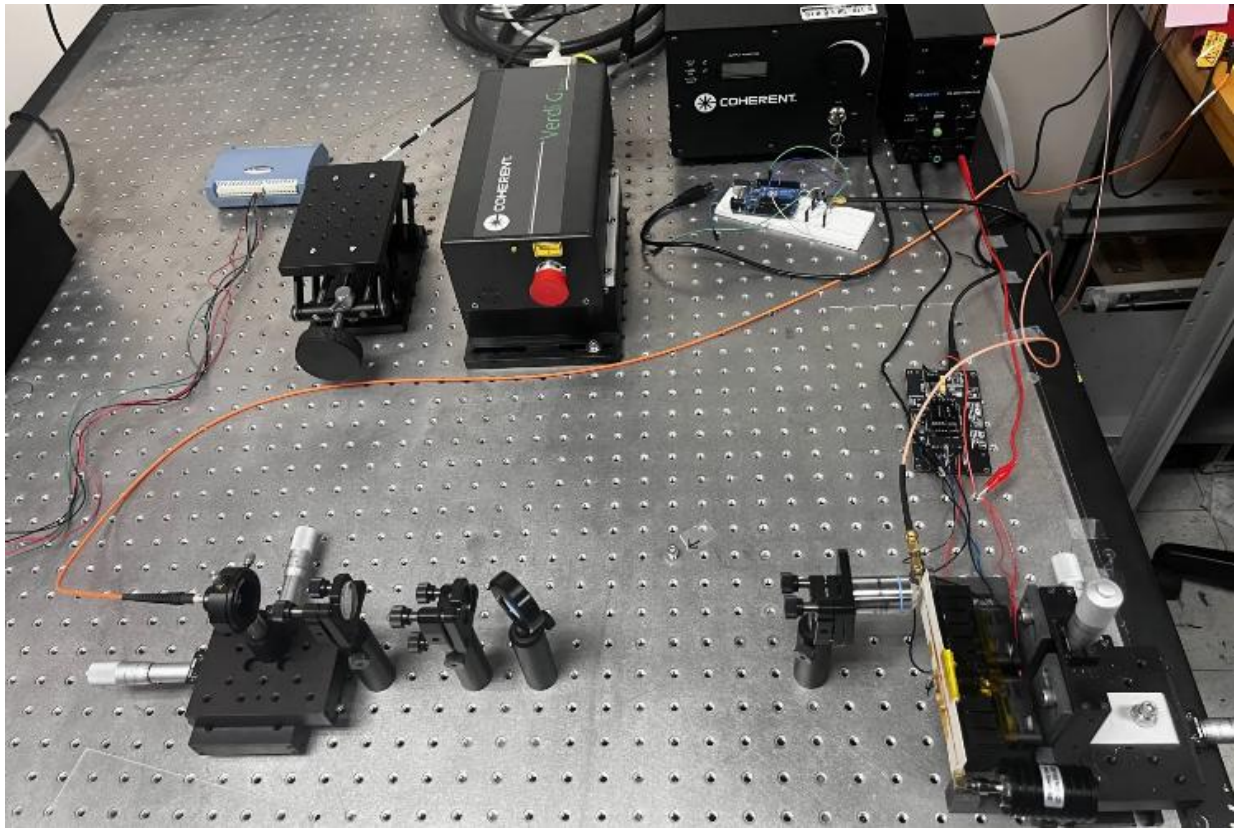

Microwave Delivery and Data Acquisition

Input (dBm)	Typical Gain (dB)	Output (dBm)	Output (W)
+7	+35	+42	16
0	+41	+41	12.6
-9	+45	+36	3.98
-18	+45	+27	0.50
-27	+45	+18	0.063

3D Printed Holder and Magnet Setup

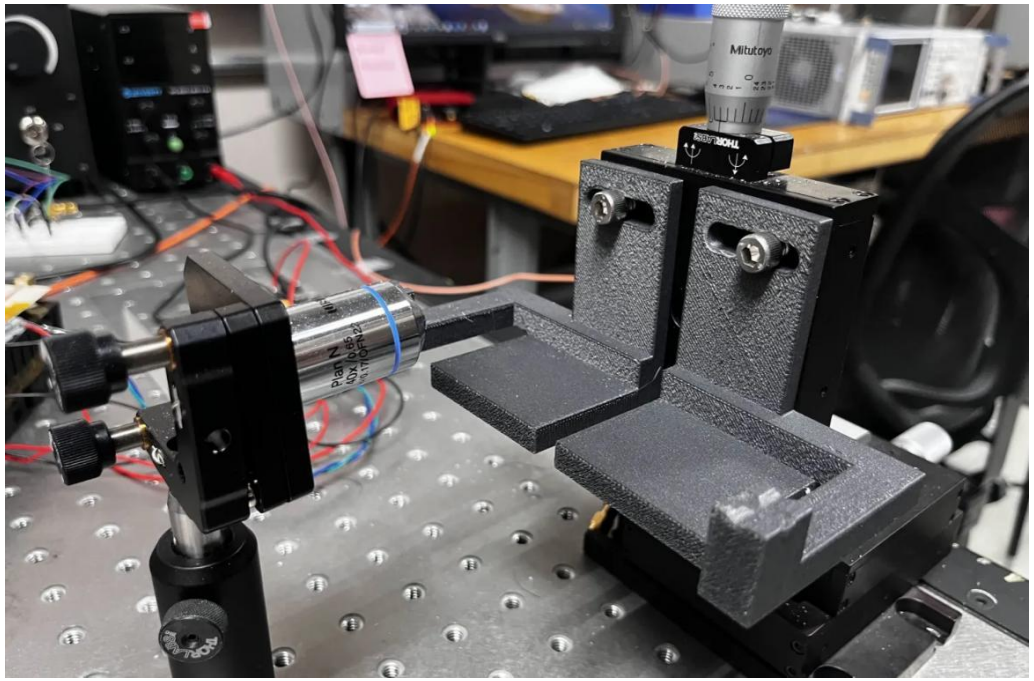

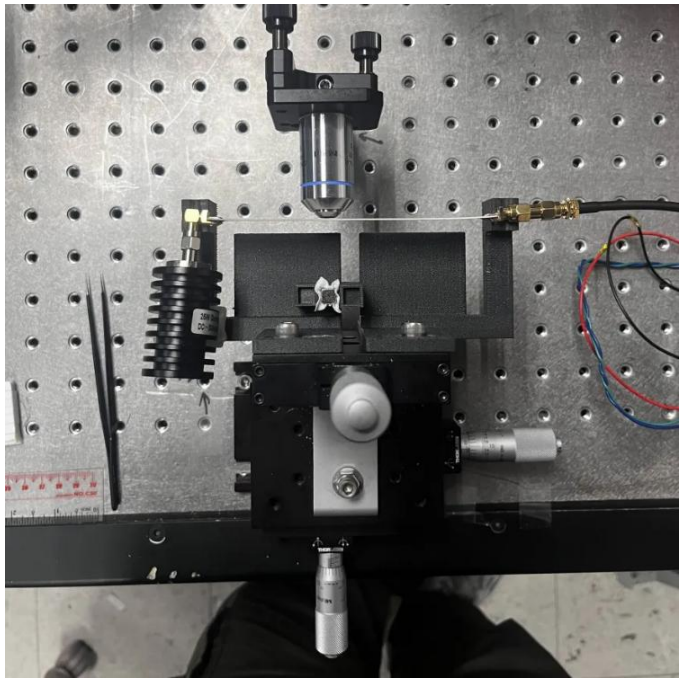

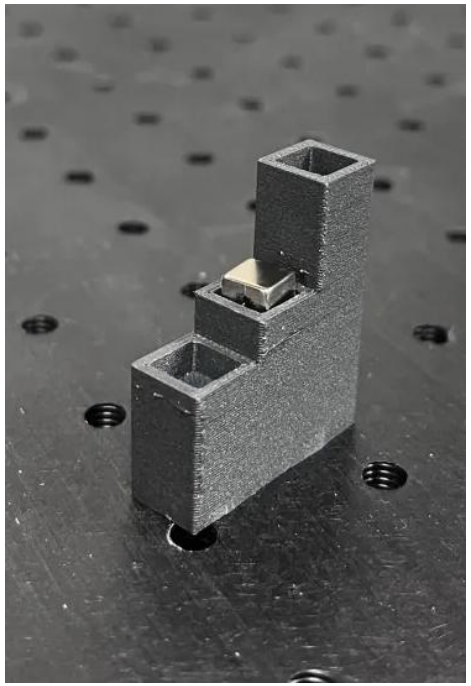

Temperature Setup

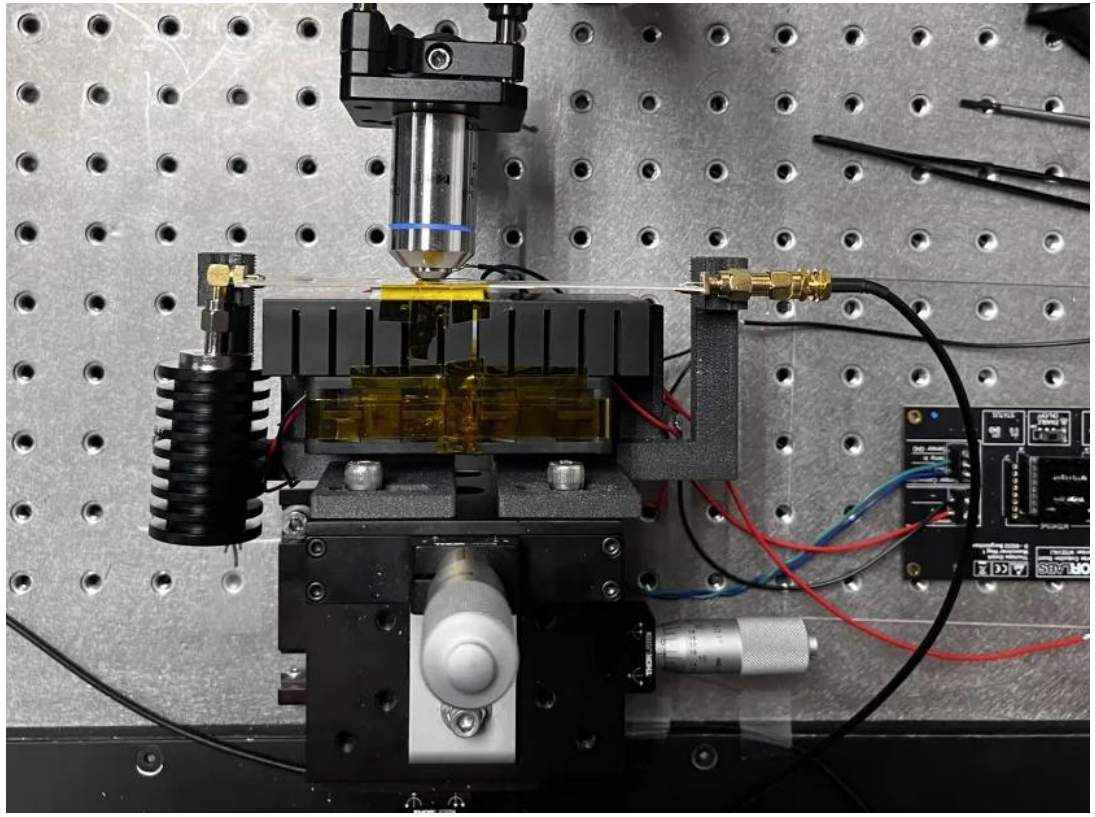

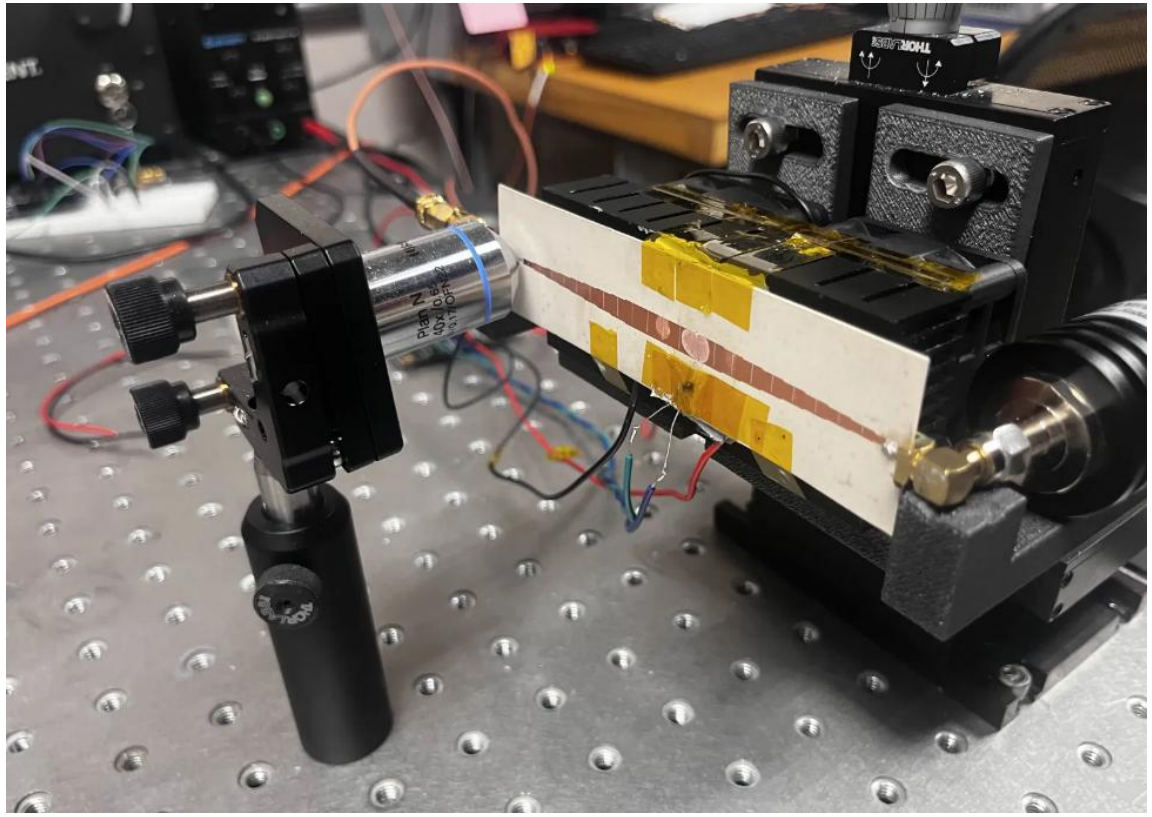

Laser Alignment Locations

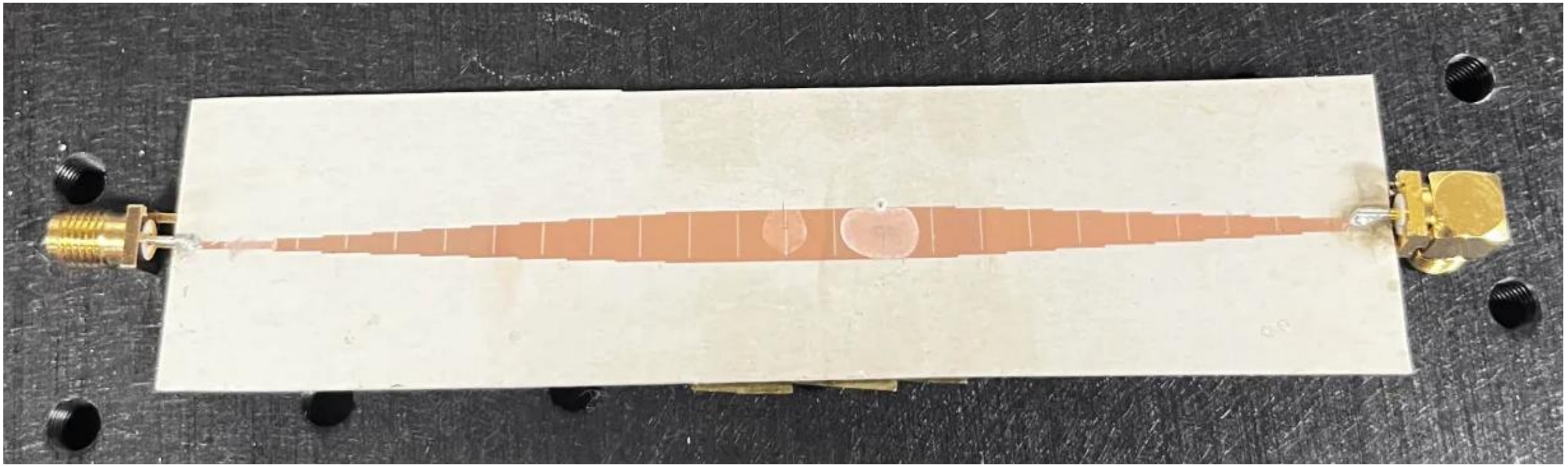

Laser Alignment Locations

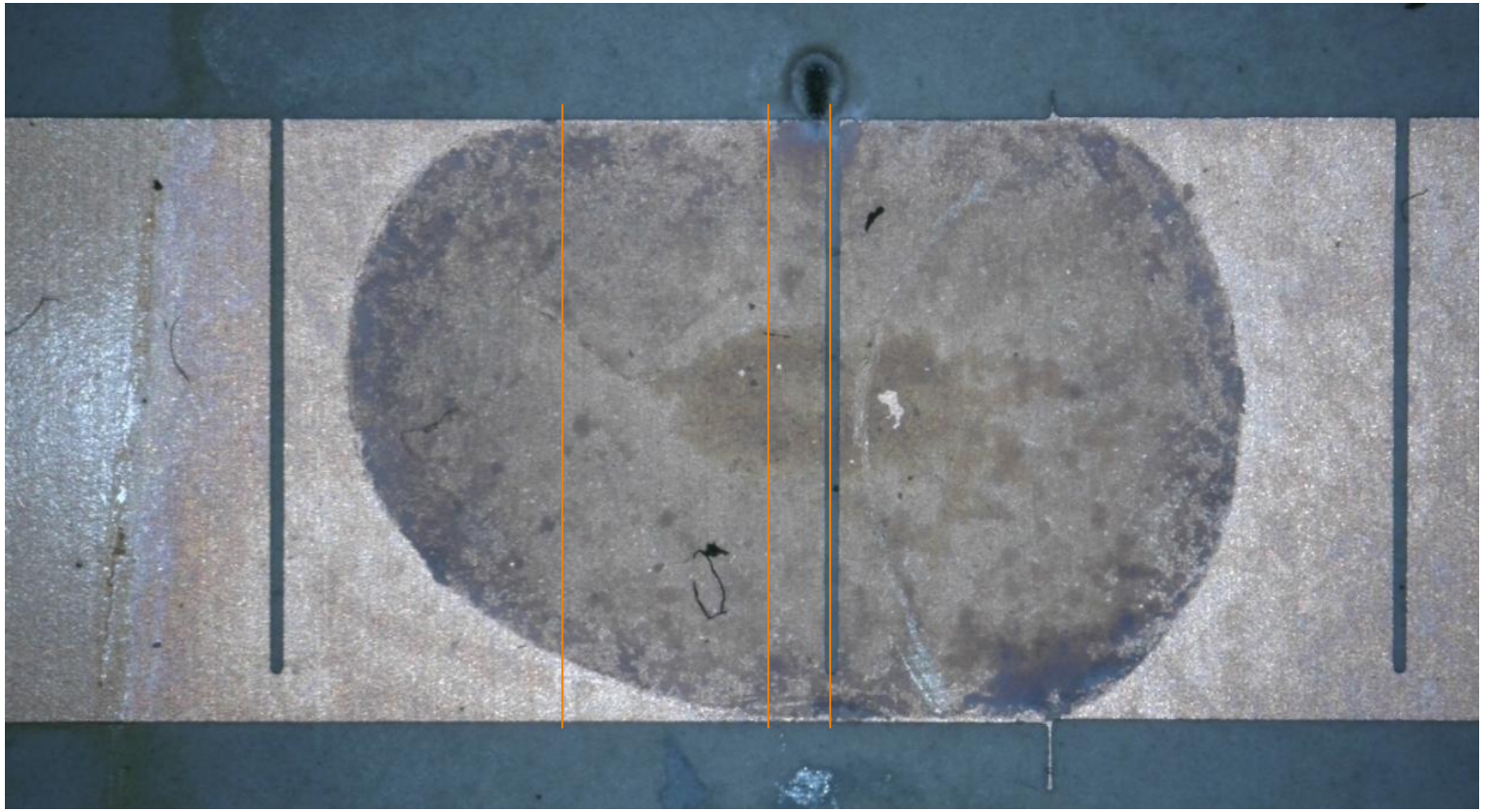

100µm Version: Baseline ODMR Plots

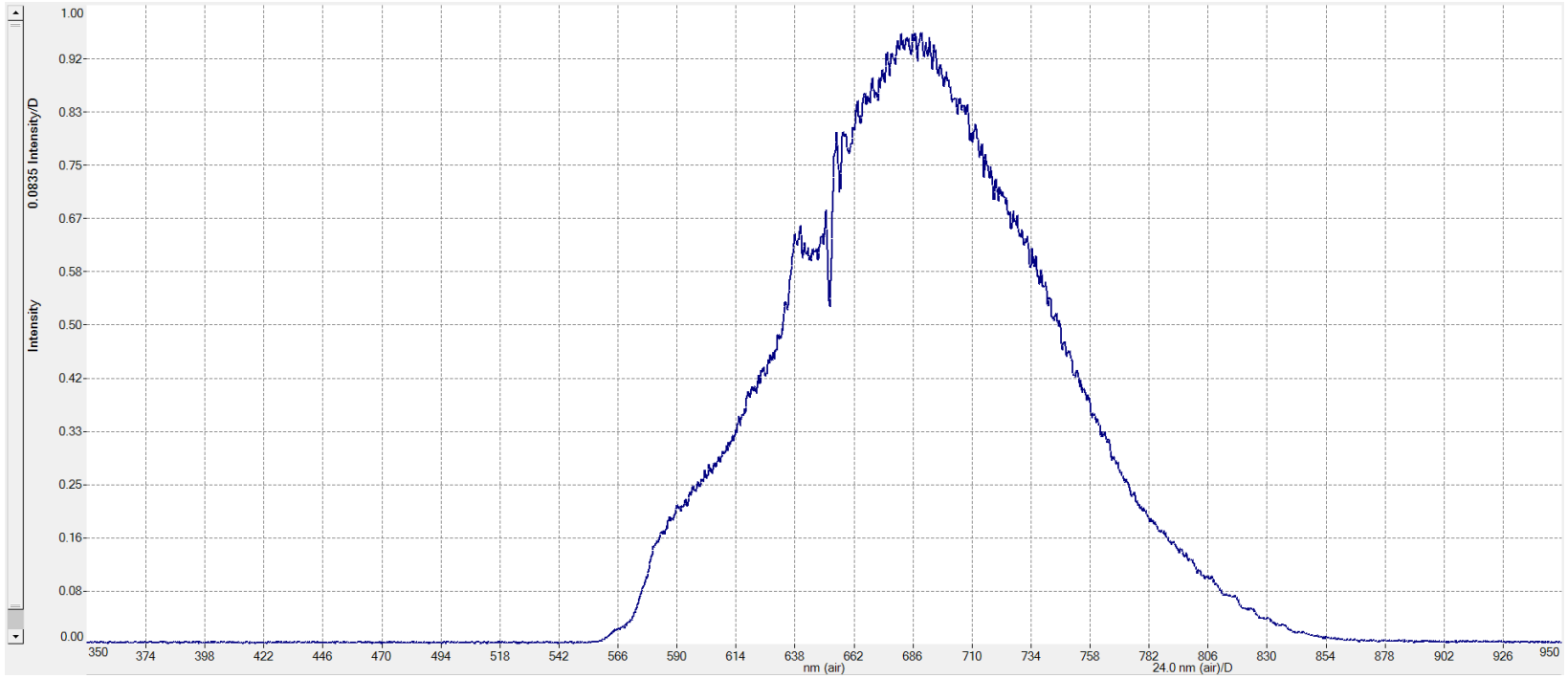

The ThorSpectra software used for ODMR to obtain fluorescence emitted by the NV centers.

100µm Version: Baseline ODMR Plots

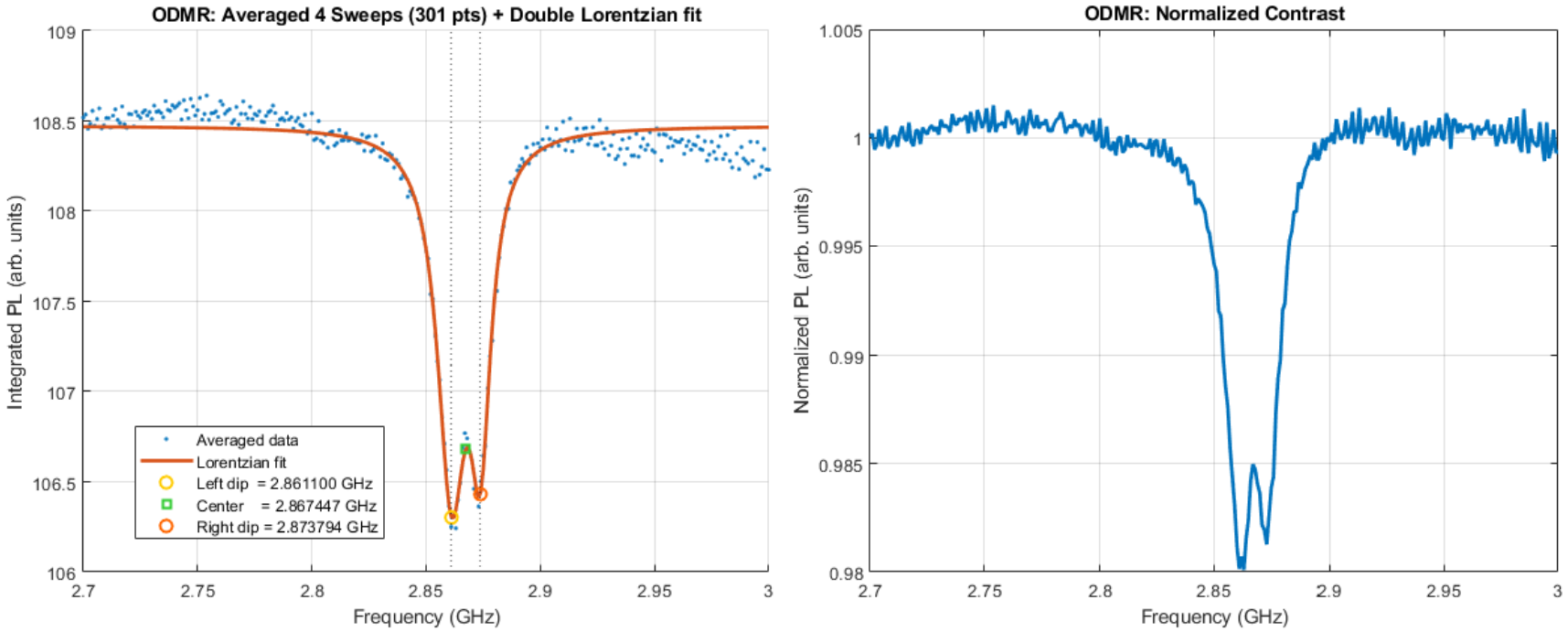

Baseline ODMR plot of the 100µm waveguide (laser pointed in between gaps, broad sweep): RF sweep from 2.7GHz – 3GHz (1MHz steps, 300 samples per period), 4 periods total at 50ms dwell time, 100mW laser power, and 7dBm RF power.

100μm Version: Varying Locations

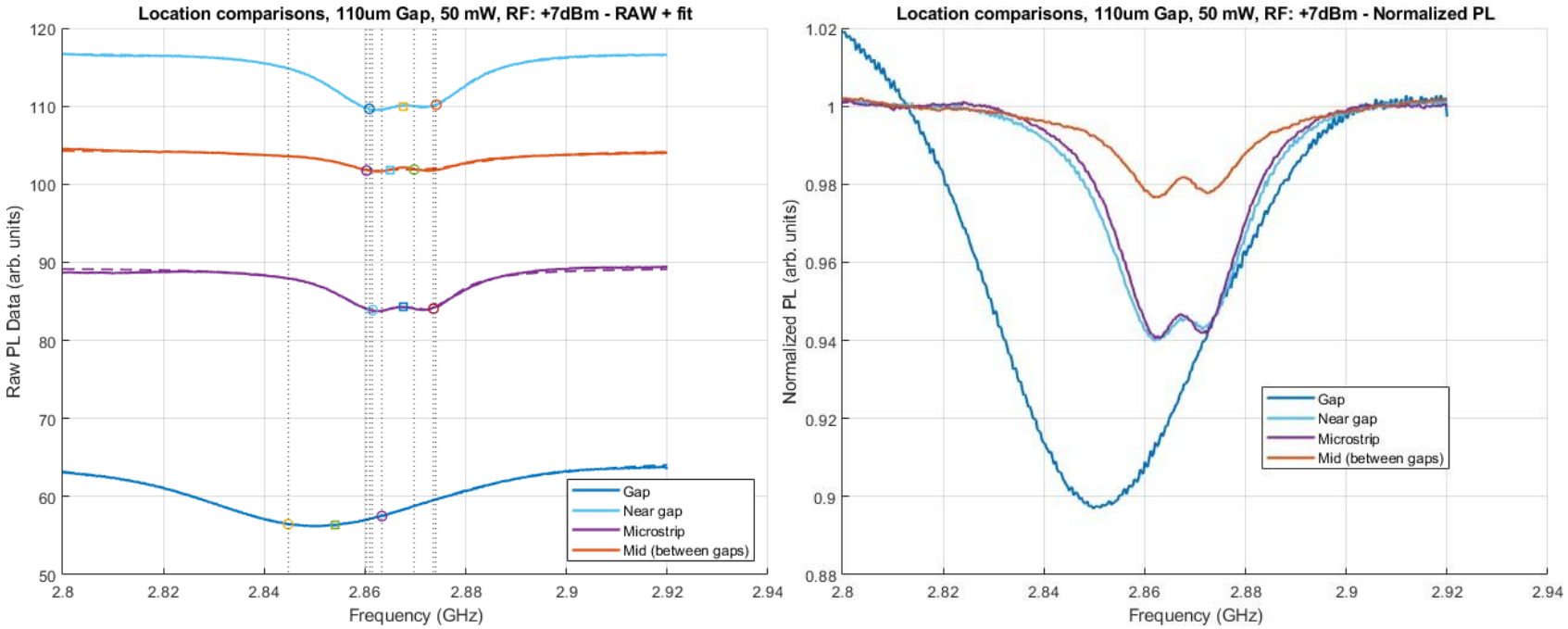

Overlayed ODMR plots of the laser being focused on 4 different locations of the 100μm waveguide: In the gap, near the gap, on the microstrip, and in between two gaps.

100μm Version: Varying Laser Power

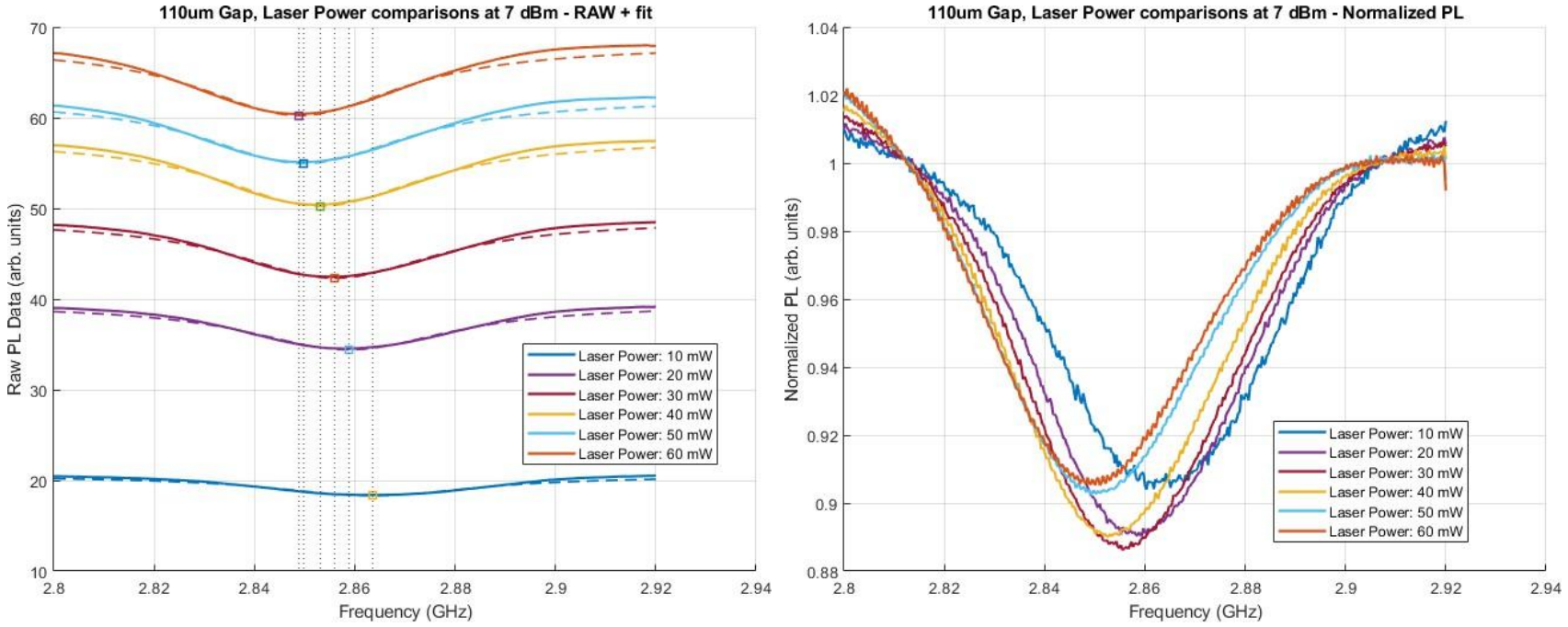

Overlayed ODMR plots to compare the contrast and resolution of ODMR data at different laser powers (focused in the 100μm gap).

100μm Version: Varying RF Power (in Gap)

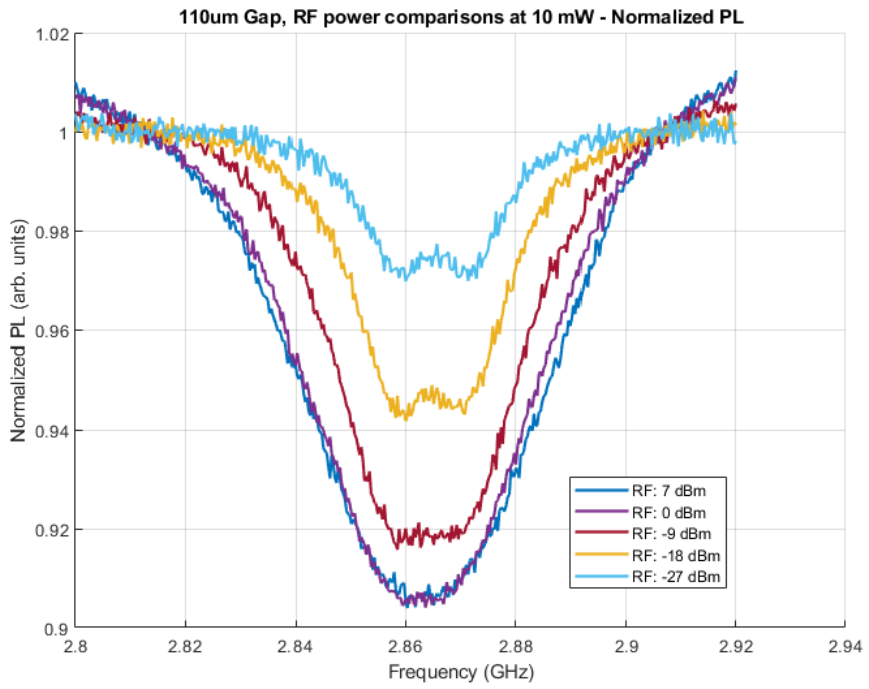

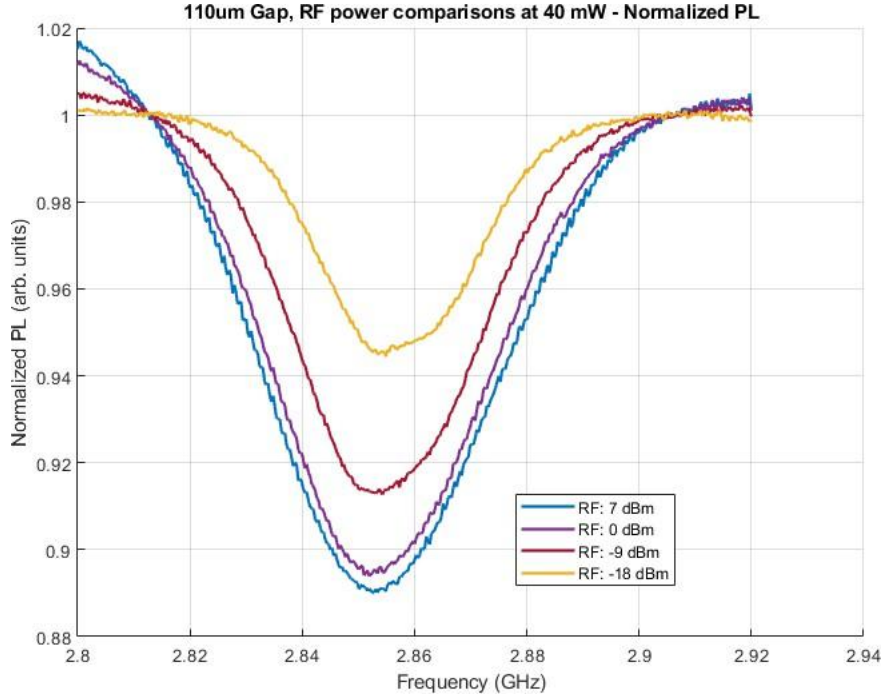

Comparison of ODMR contrast and resolution at different RF power at a stable 10mW and 40mW laser power (focused in the 100μm gap).

100µm Version: Varying RF Power (between gaps)

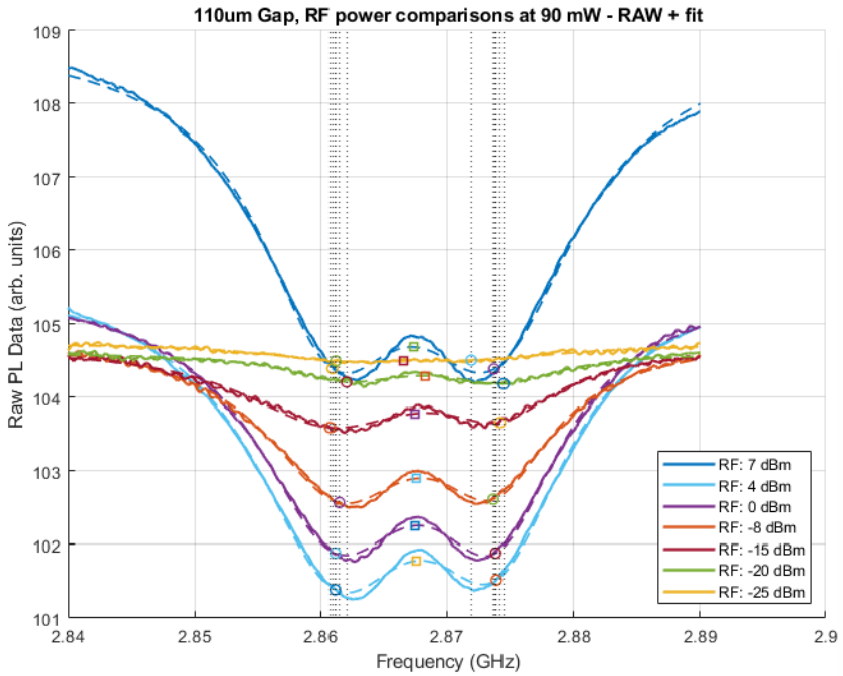

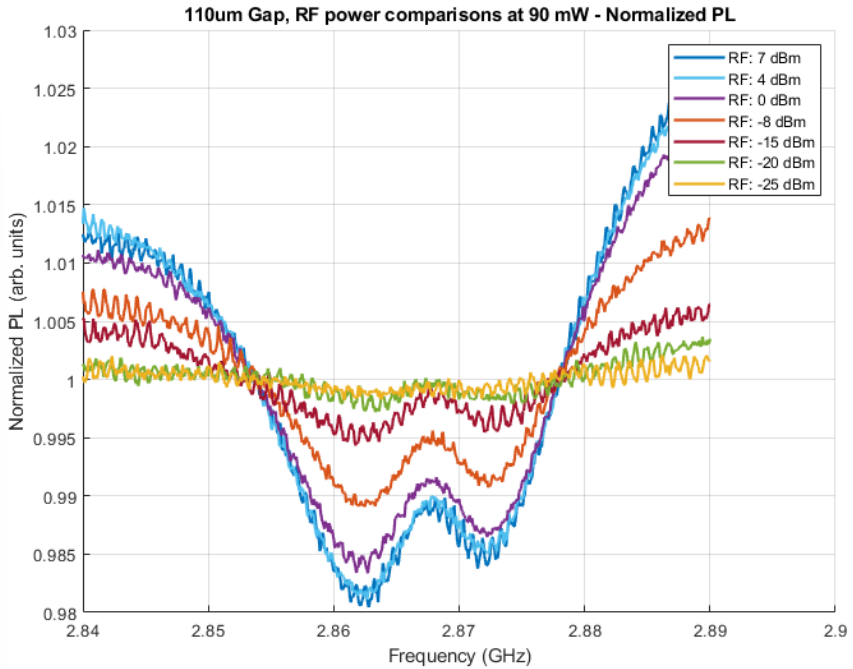

Overlayed plots to compare the contrast and resolution of ODMR data at different RF power at a stable 90mW laser power (focused near the 100µm gap).

100μm Version: Varying Magnetic Fields

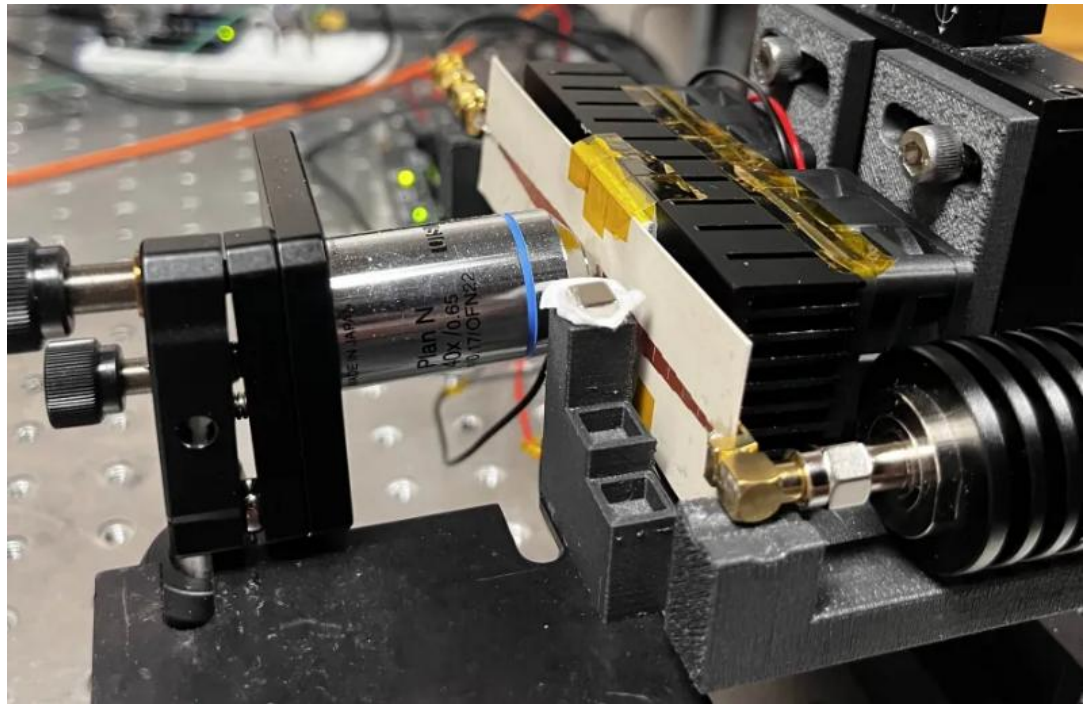

Placement of the magnet next to the waveguide of varying distances, measured using a ruler from top-down view.

100µm Version: Varying Magnetic Fields

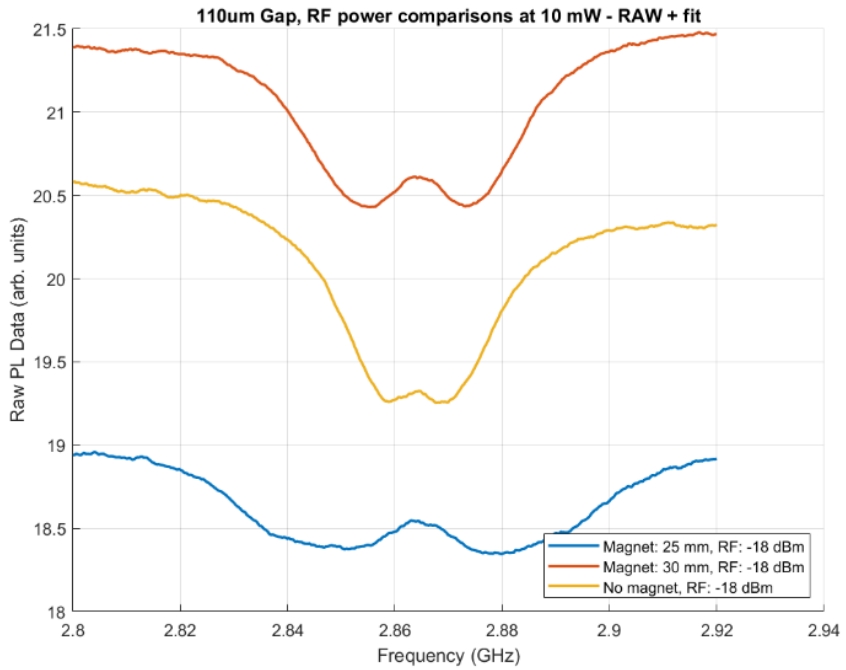

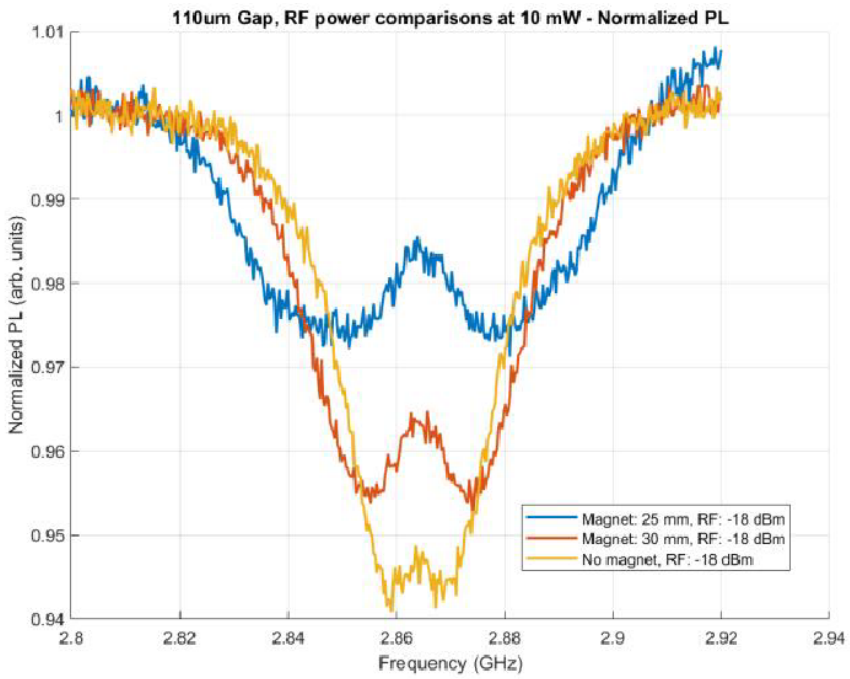

Overlayed plots to compare the contrast and Zeeman splitting of ODMR data at different RF power at a stable 10mW laser power at varying magnet locations (in the 100µm gap).

100µm Version: Varying Magnetic Fields

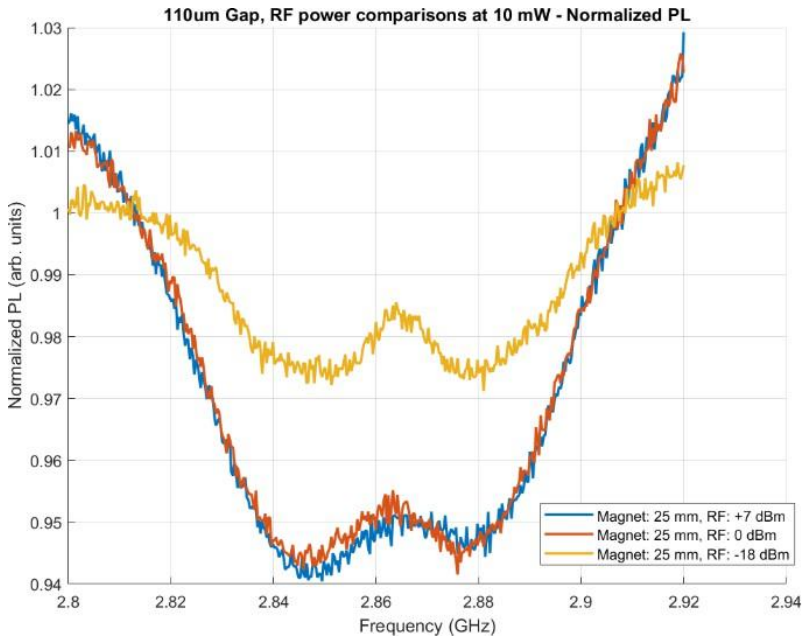

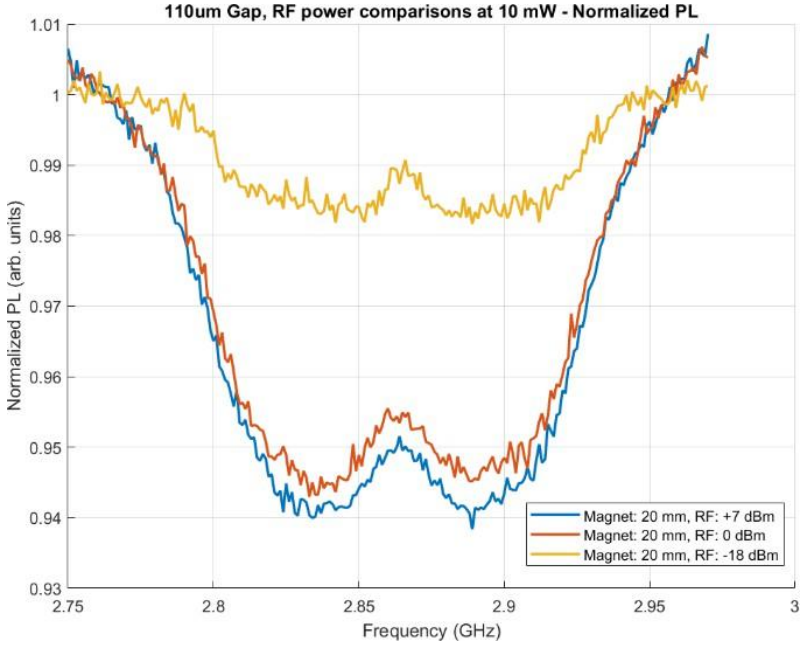

Overlayed plots to compare the contrast and Zeeman splitting of ODMR data at different RF powers at a stable 10mW laser power at varying magnet locations (in the 100µm gap).

100µm Version: Thermal Testing

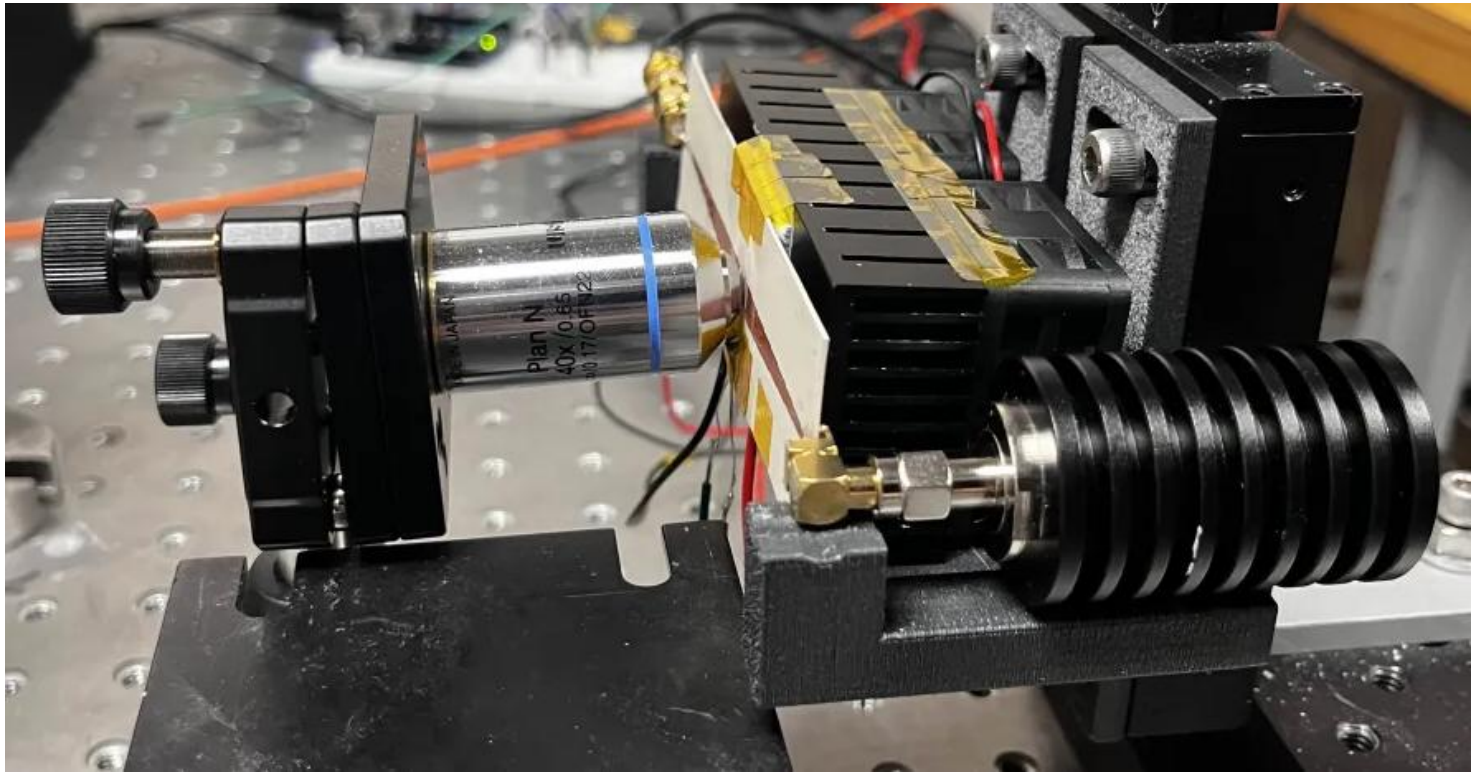

100µm Version: Thermal Testing

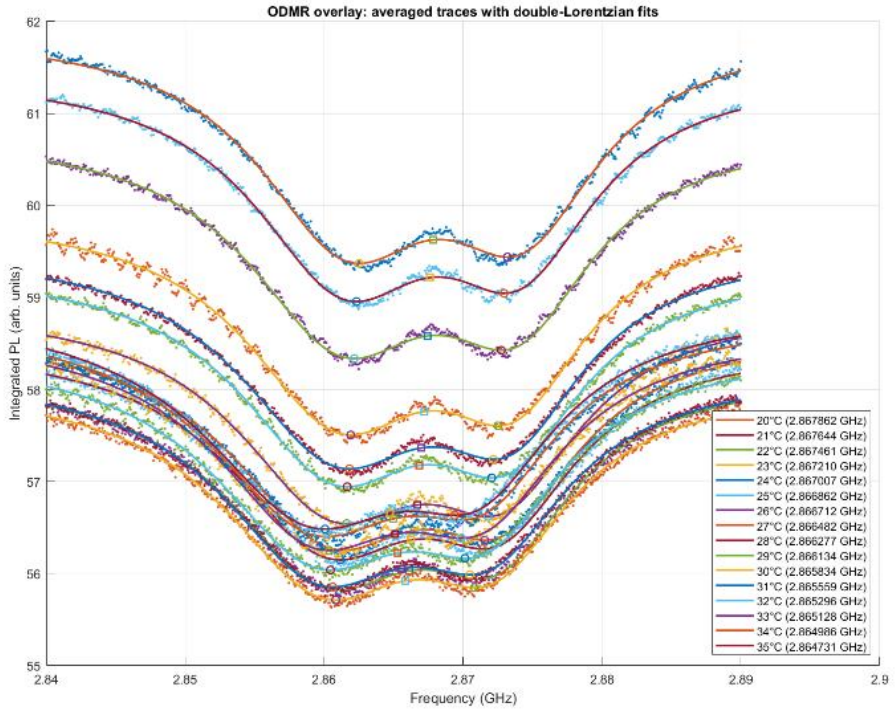

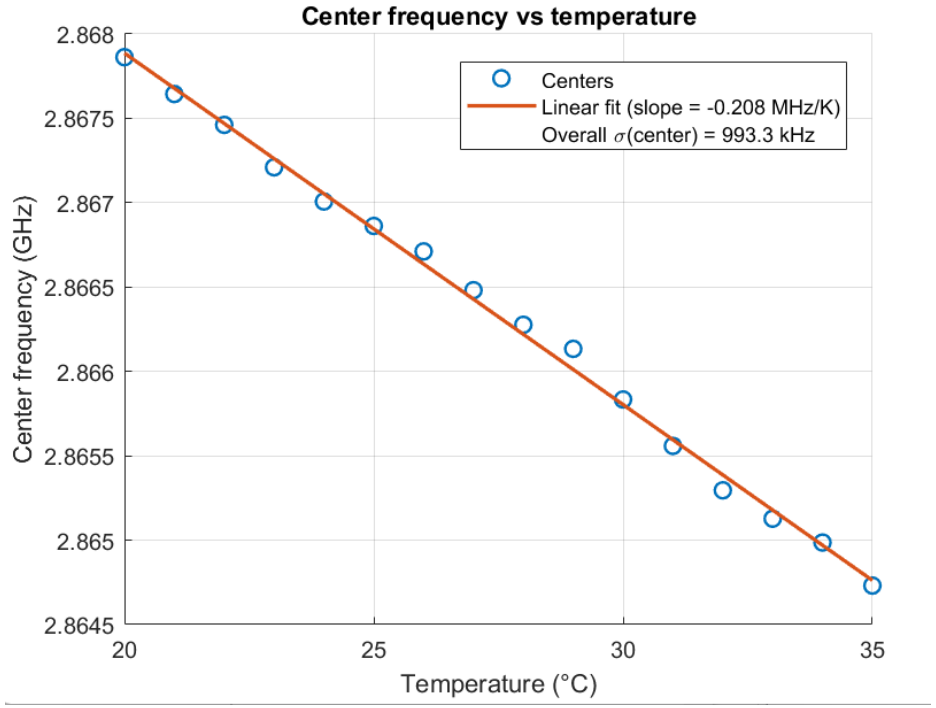

Overlayed plots to compare fluorescence levels and analyze the trend in center frequency shifting caused by thermal effects with laser power at 150mW (20ms dwell time).

100µm Version: Thermal Testing

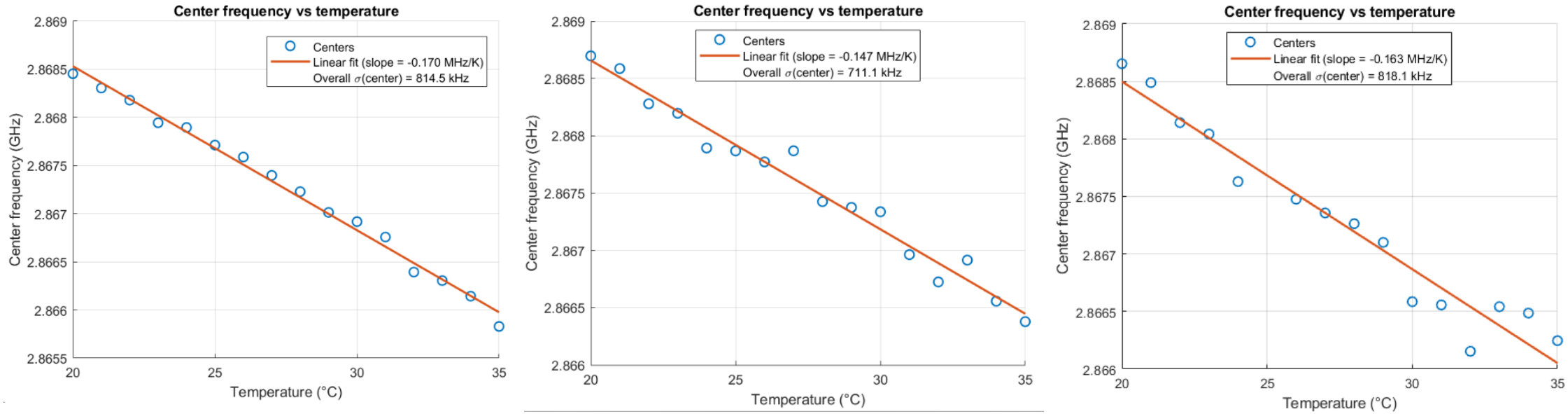

A repeat of the plots from Figure 7.14, but with varying laser power and dwell time per row. **Left:** Laser intensity at 90mW (40ms dwell time). **Middle:** Laser intensity at 70mW (50ms dwell time). **Right:** Laser intensity at 50mW (50ms dwell time).

100µm Version: Thermal Testing

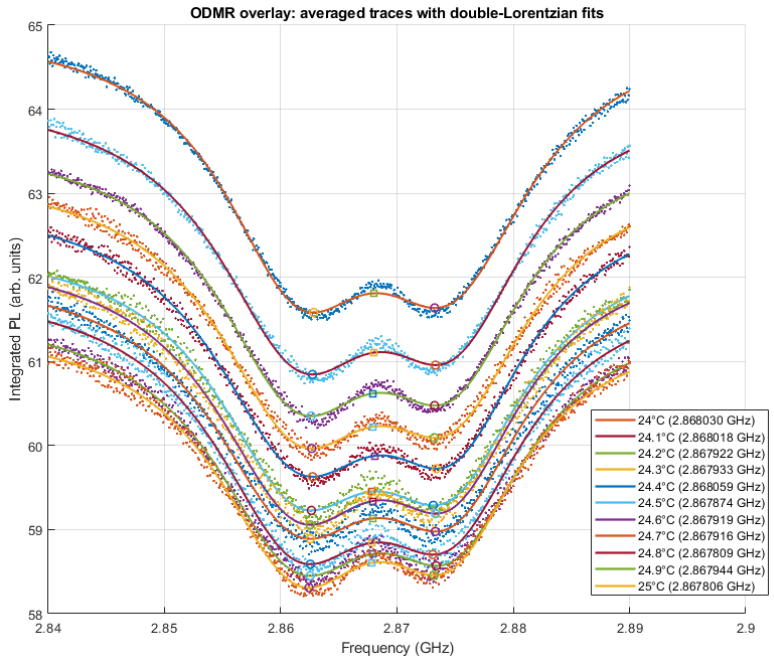

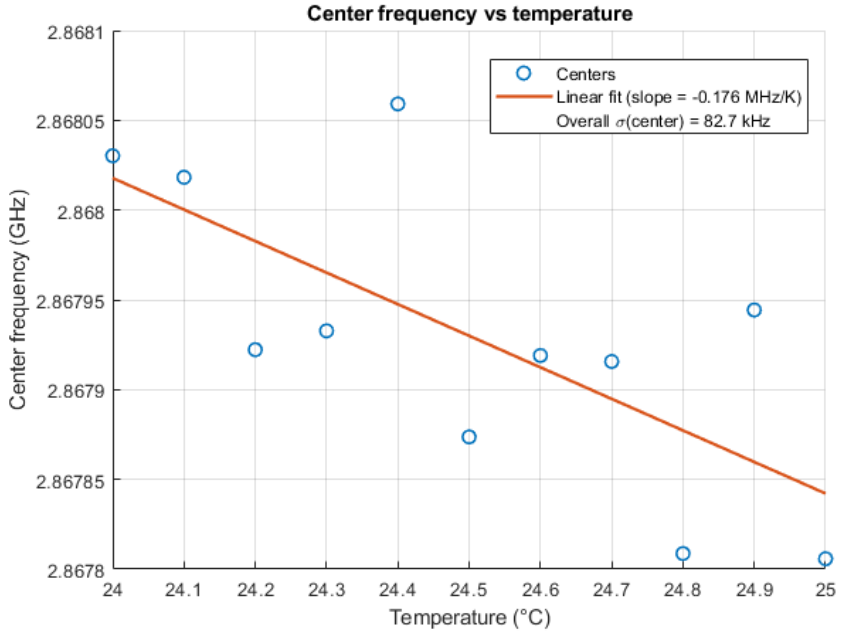

A repeated temperature sweep with smaller temperature steps (0.1°C) at a narrower range (24°C – 25°C) to determine more precise temperature resolution at 50mW laser intensity (50ms dwell time).

100μm Version: Thermal Testing

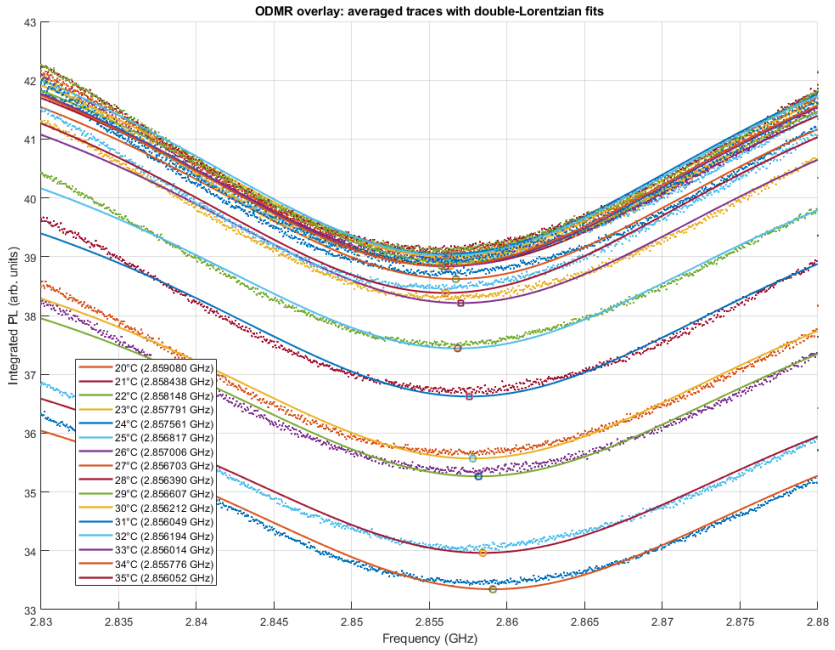

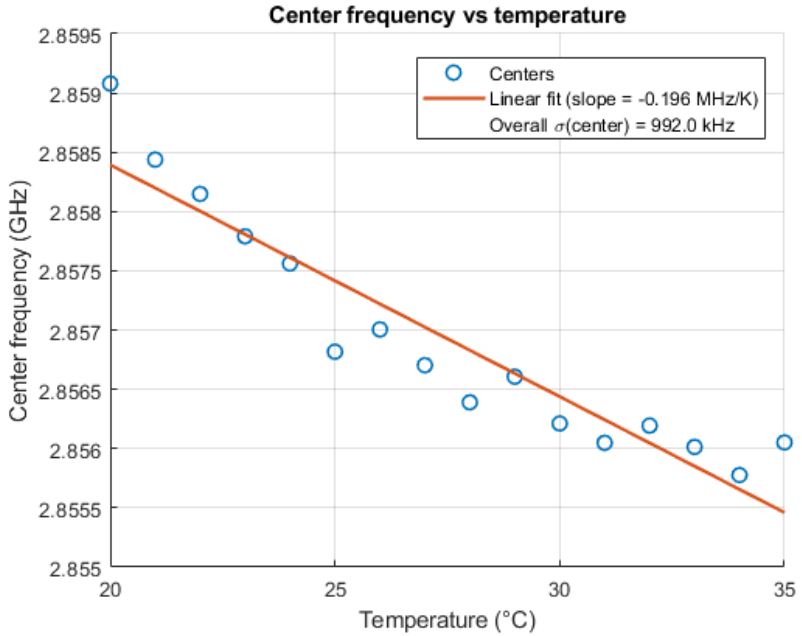

A repeated broad temperature sweep with the laser focused in the 100μm gap of the waveguide at 30mW laser power (50ms dwell time).

100μm Version: Thermal Testing

Laser Power (mW)	Laser Location	Sweep Type	Slope (kHz/K)	Estimated Temperature Range (°C)	ΔT (°C)
150	Near gap	Broad	-200	53.0 – 89.5	42.5
90	Near gap	Broad	-170	41.7 – 77.1	35.4
70	Near gap	Broad	-147	38.0 – 69.2	31.2
50	Near gap	Broad	-163	40.0 – 71.3	31.3
50	Near gap	Narrow	-176	47.3 – 50.3	3.0
30	In gap	Broad	-196	148.8 – 189.7	40.9

$$\frac{35.1°C\ \Delta T_{NV\ Center}}{16°C\ \Delta T_{TEC\ Controlled}}$$

$$\approx \frac{2.2°C\ \Delta T_{NV\ Center}}{1°C\ \Delta T_{TEC\ Controlled}}$$

Summary of all the test runs during thermal testing, as discussed in this section

100µm Version: Thermal Testing

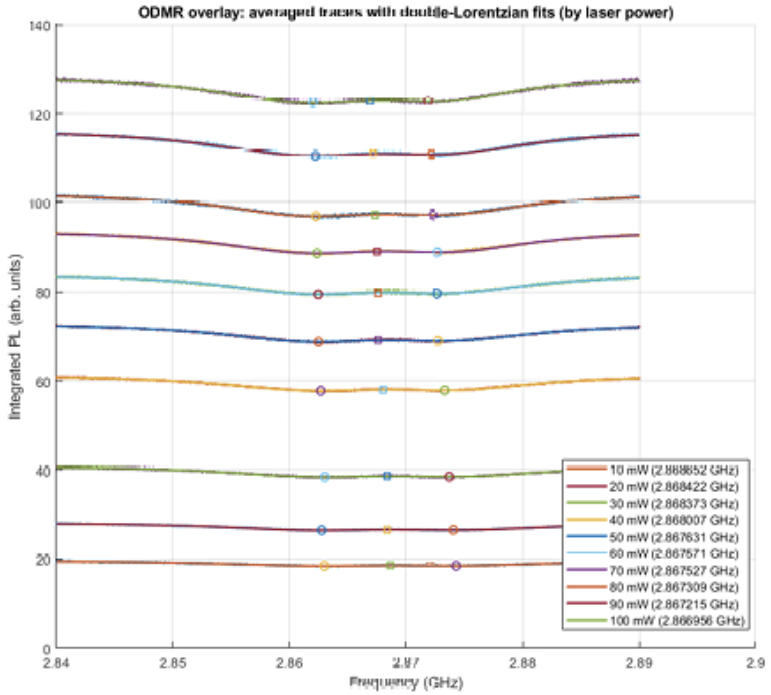

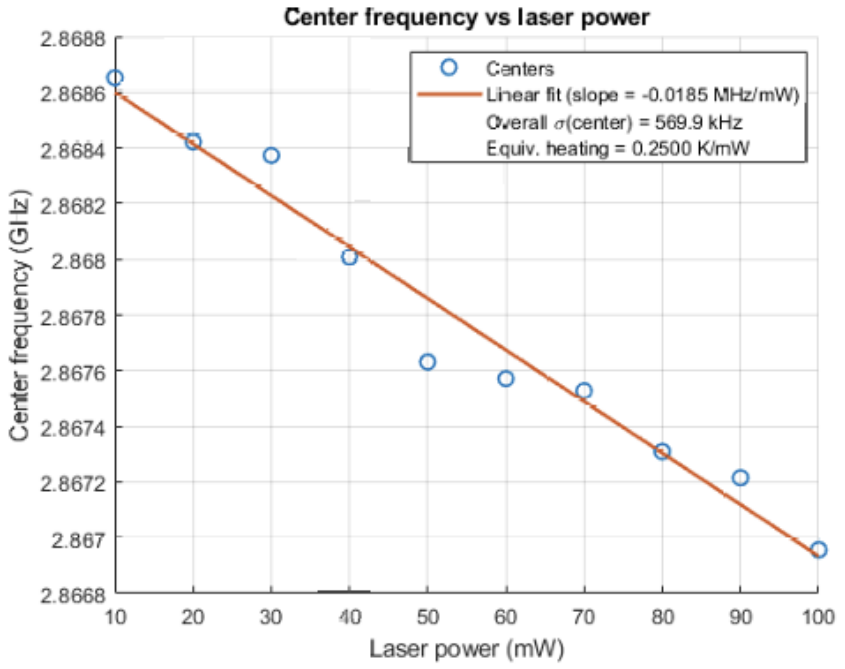

$$Equivalent\ Heating$$

$$= \frac{Linear\ fit}{NV\ thermal\ coefficient}$$

$$= \frac{-18.5 kHz/mW}{-74 kHz/K}$$

$$= 0.25\ K/mW$$

Laser intensity sweep done with the TEC at a stable 25°C (near gap)

200µm and 300µm Version: Baseline ODMR Plots

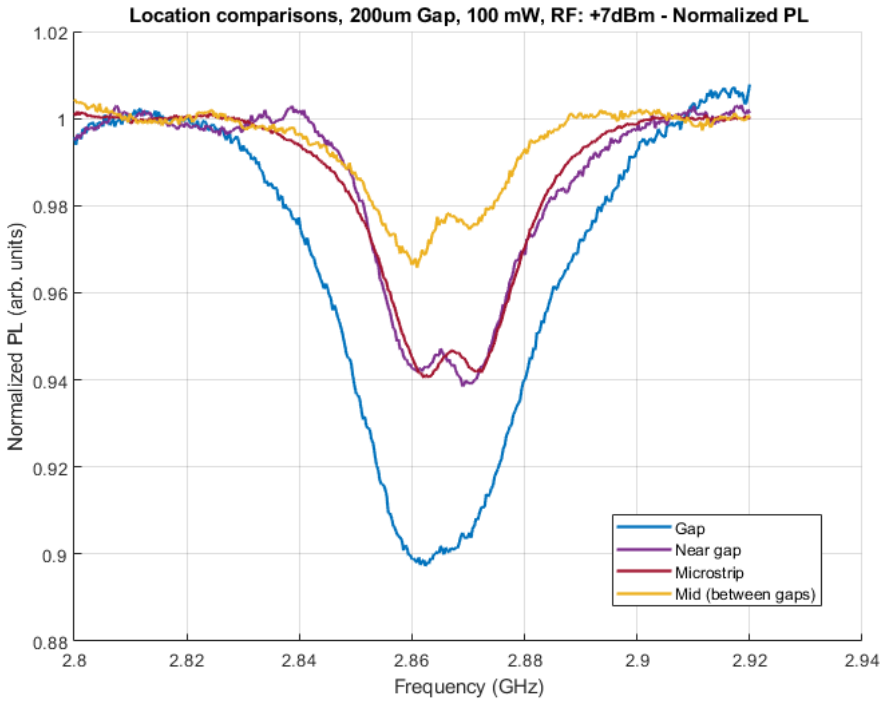

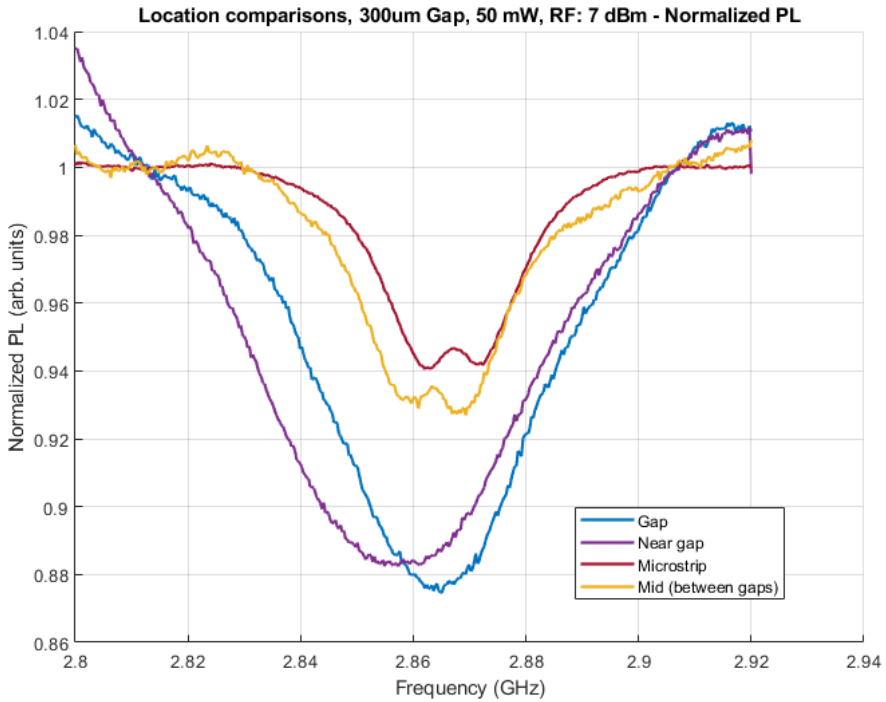

Overlayed ODMR plots with varying laser locations to compare contrast (200µm and 300µm)

200μm Version: Varying RF Power

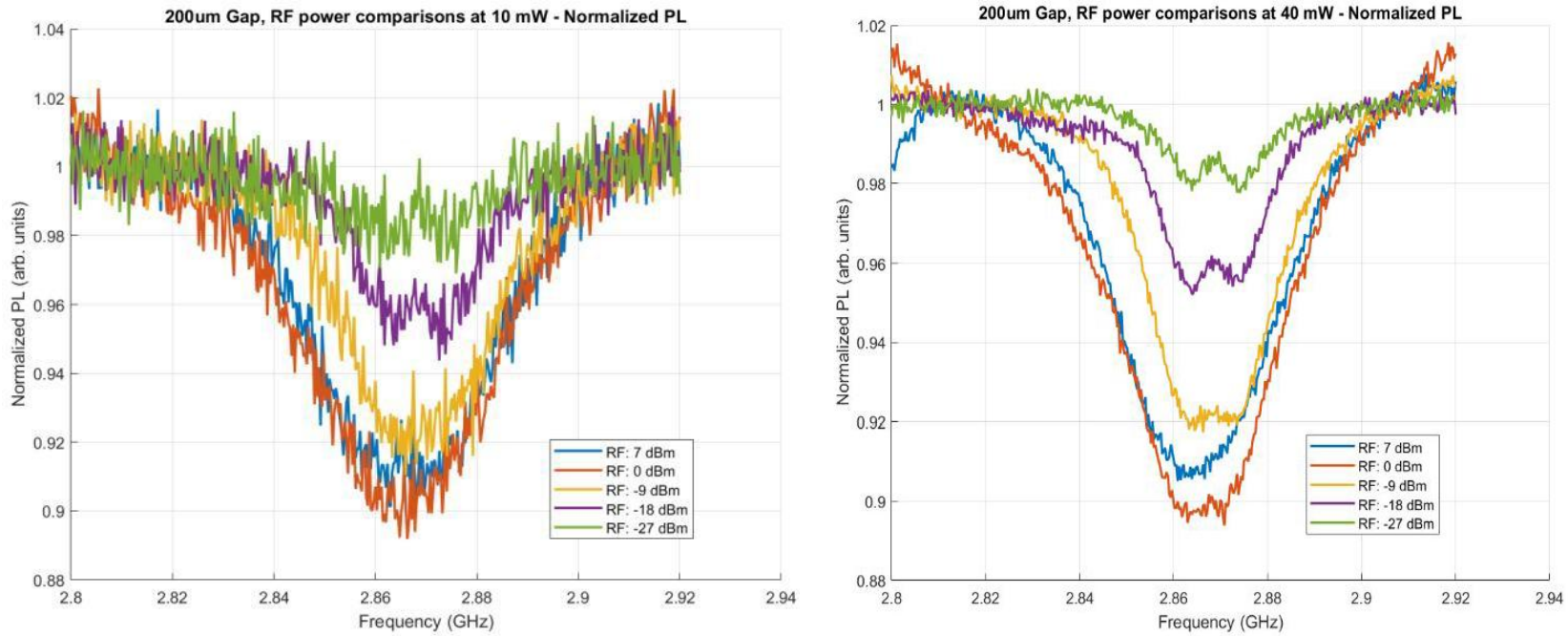

Overlayed ODMR plots with varying RF powers at two laser intensities (200μm).

300μm Version: Varying RF Power

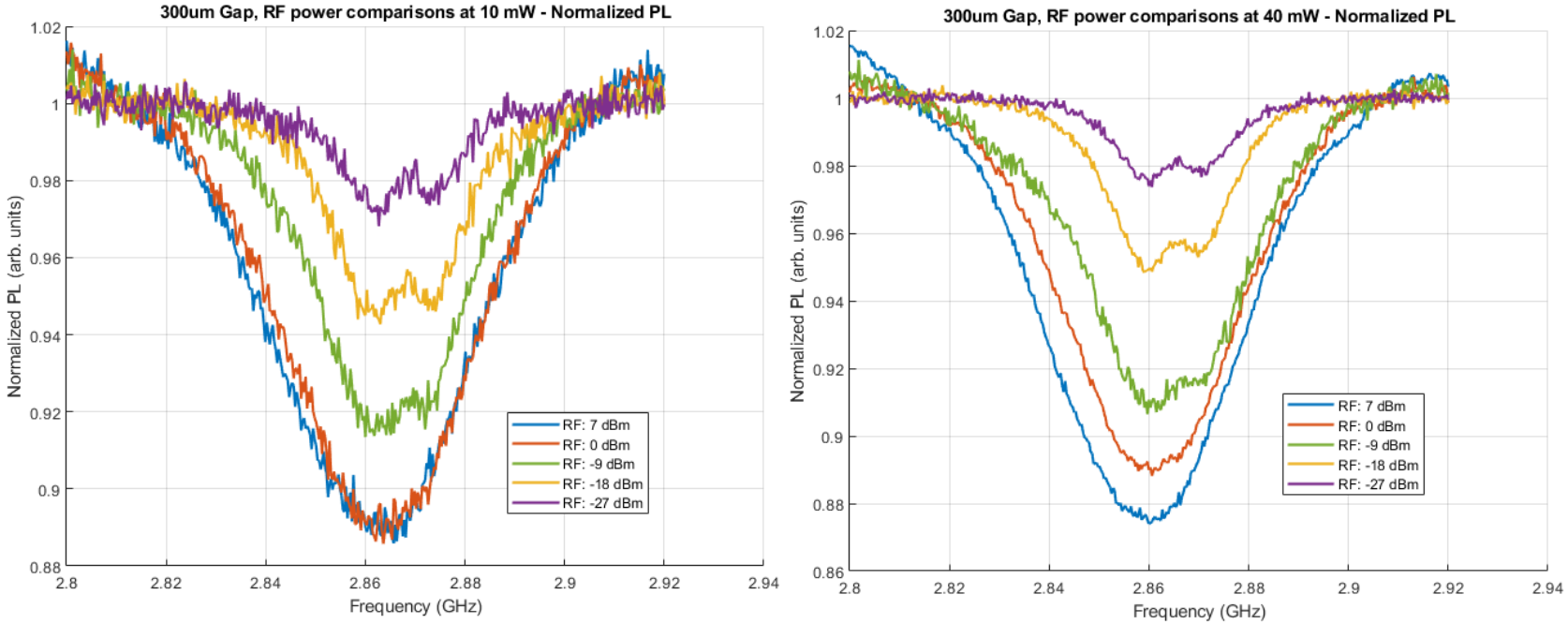

Overlayed ODMR plots with varying RF powers at two laser intensities (300μm).

200μm and 300μm Version: Varying Magnetic Fields

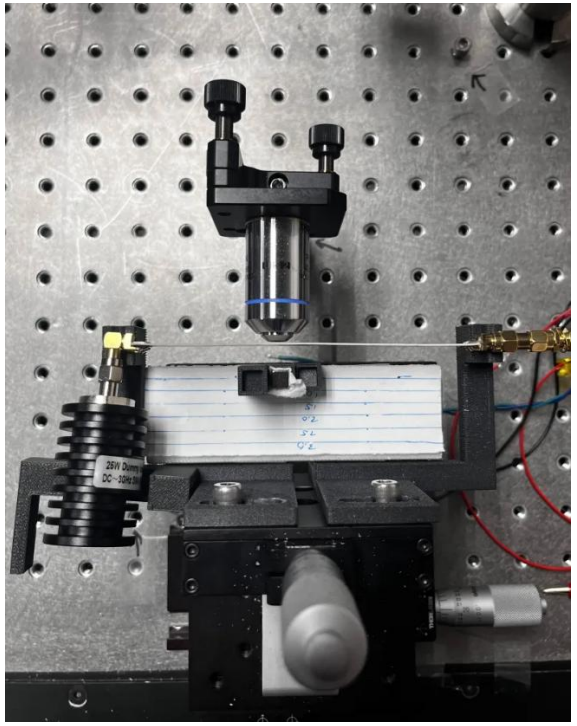

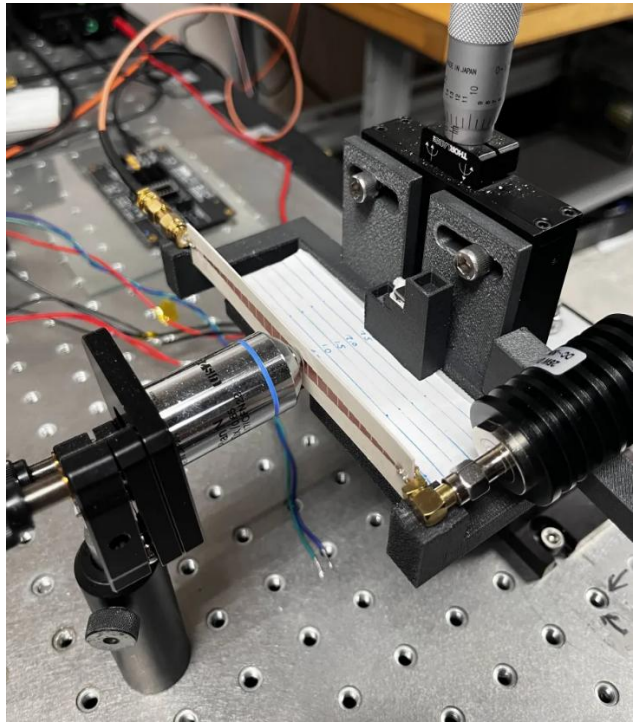

Setup for magnet placement

200µm Version: Varying Magnet Locations

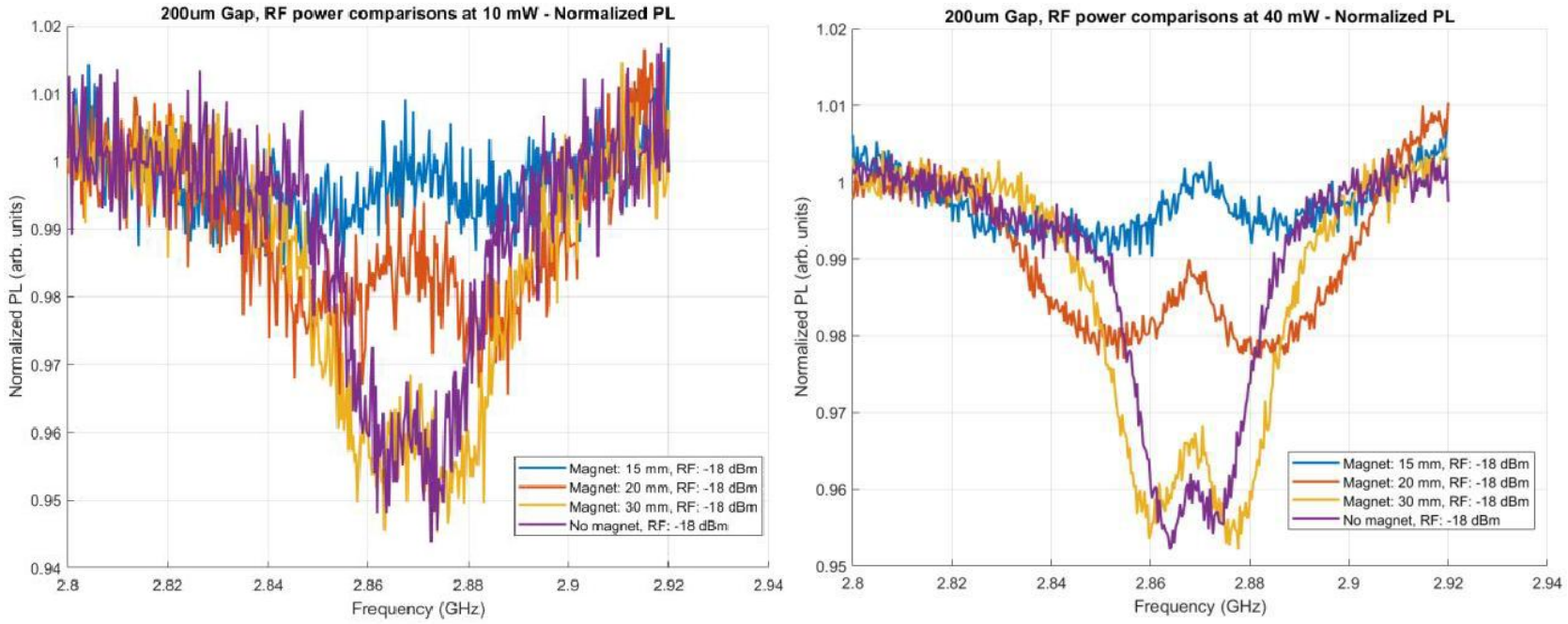

ODMR plots of different magnet distances at a stable RF input power of -18dBm (200µm, in gap)

300µm Version: Varying Magnet Locations

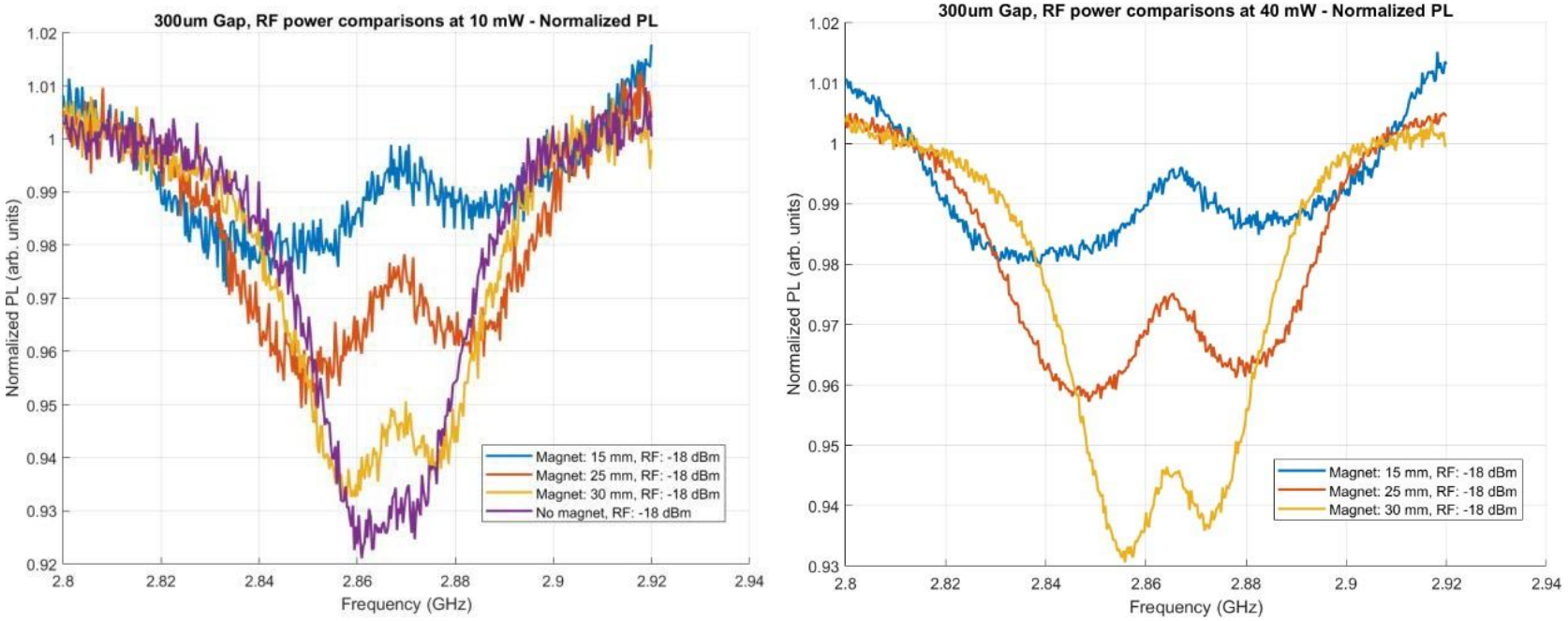

ODMR plots of different magnet distances at a stable RF input power of -18dBm (300µm, in gap)

300µm Version: Varying Magnet Locations

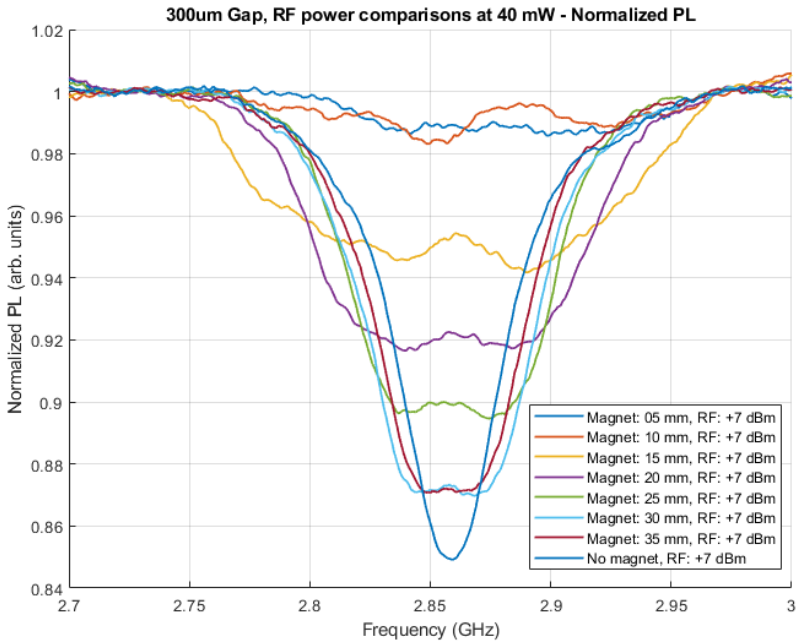

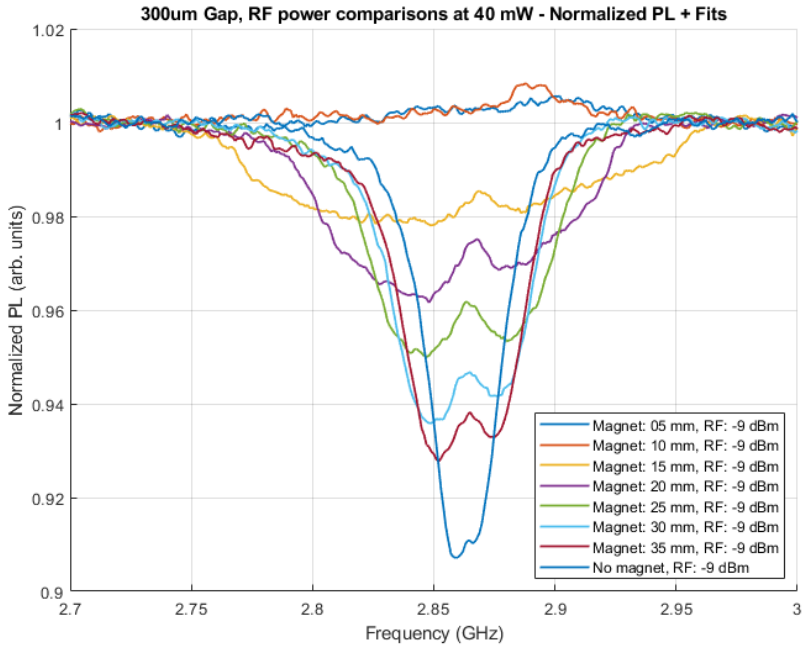

ODMR plots of different magnet distances at two RF input powers. **Left:** 7dBm and **Right:** -9dBm, both at 50mW laser power (300µm, in gap)

300μm Version: Varying Magnet Locations

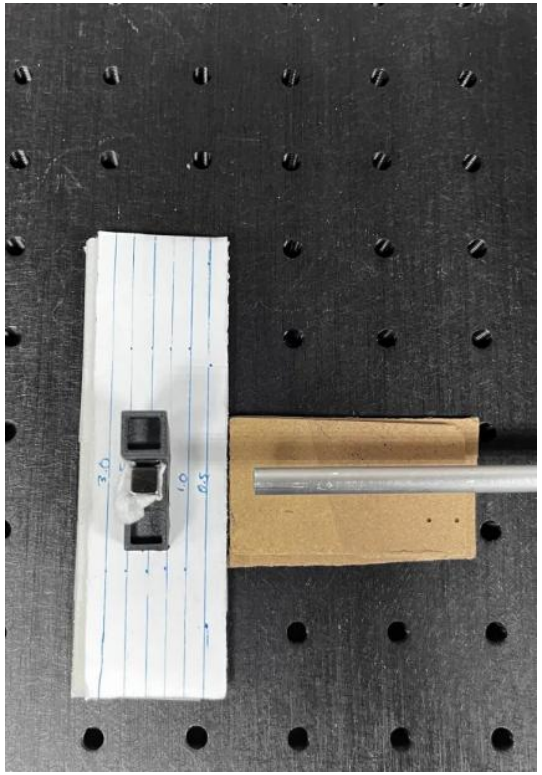

Gaussmeter setup

300μm Version: Varying Magnet Locations

Magnet Distance (mm)	Δf (MHz)	ODMR Mag Field (mT)	Measured Field (mT)
35	2.851 – 2.874 = 23	0.41	0.64
30	2.849 – 2.876 = 27	0.48	1.06
25	2.845 – 2.882 = 37	0.66	1.60
20	2.833 – 2.892 = 59	1.05	2.56
15	2.819 – 2.907 = 88	1.57	4.48

Magnetic field calculations from ODMR plot (-9dBm) vs. measured field from gaussmeter

$$\Delta f = 2\gamma B_z$$

$\Delta f = frequency\ separation\ between\ dips$

$\gamma = NV\ gyromagnetic\ ratio \approx 28GHz/T$

$B_z = magnetic\ field\ along\ the\ NV\ axis$

$$= \frac{\Delta f}{2\gamma} = \frac{\Delta f}{2 \cdot 28GHz}$$

Microstrip ODMR Plot: Re-run

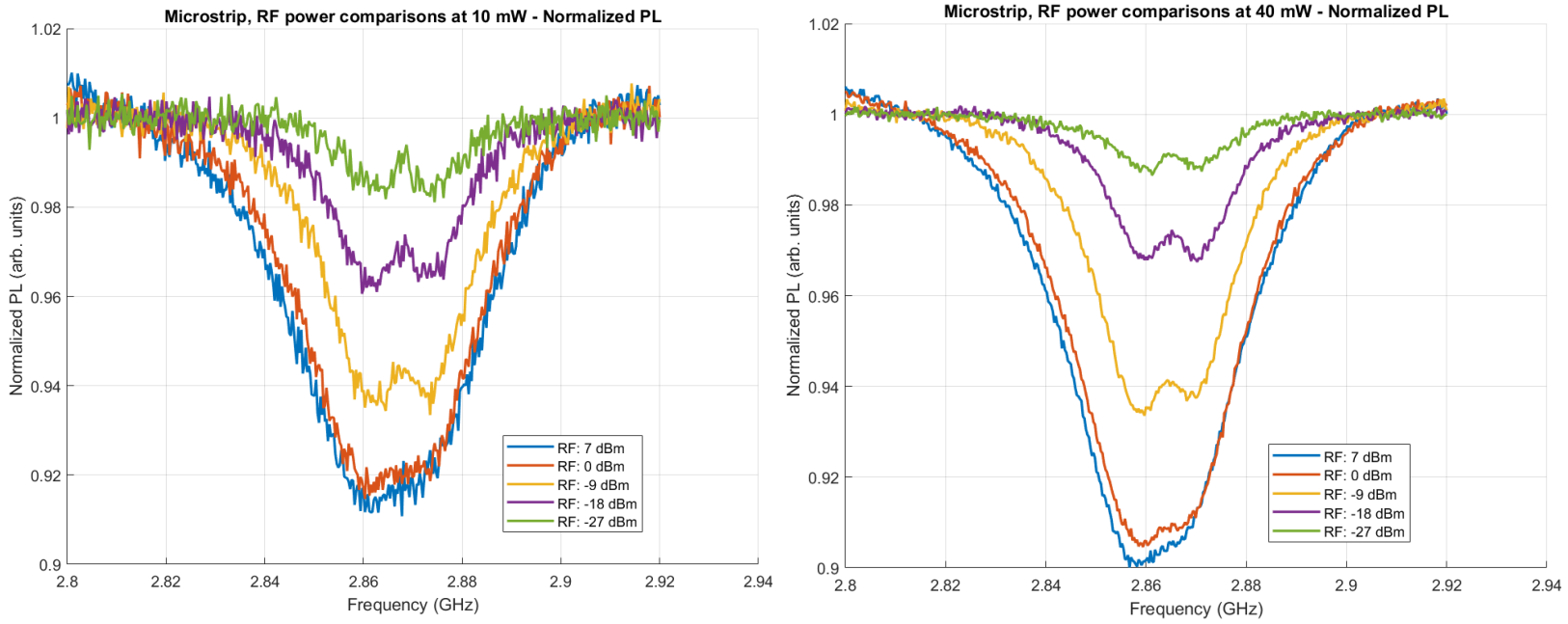

Overlayed ODMR plots with varying RF powers at 10mW laser intensity (100µm version, microstrip region).

Post-Fabrication Simulations

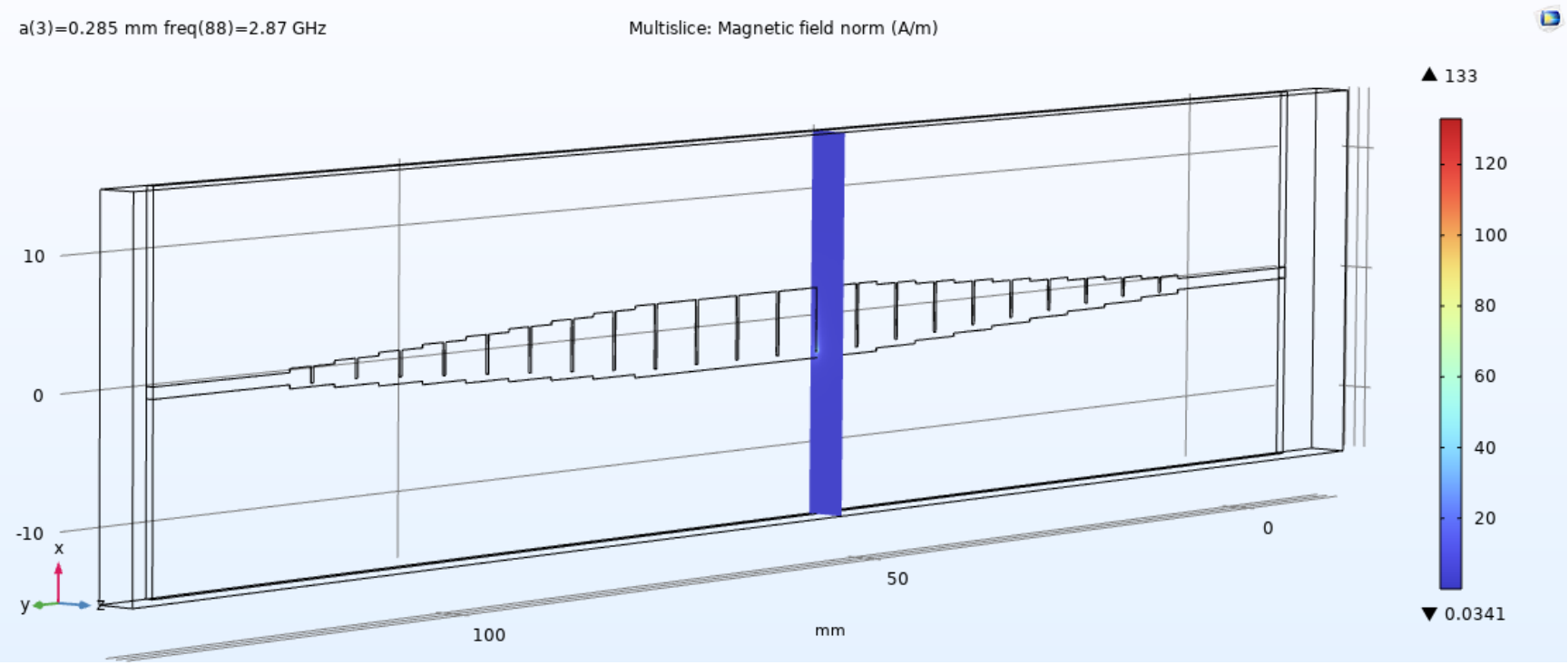

Simulation of the XZ-plane used to measure magnetic field norm in the gap (A/m).

Post-Fabrication Simulations

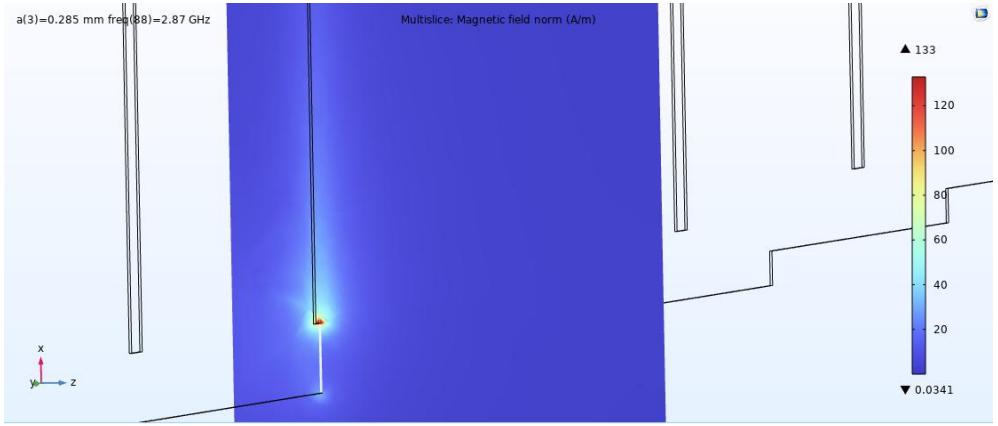

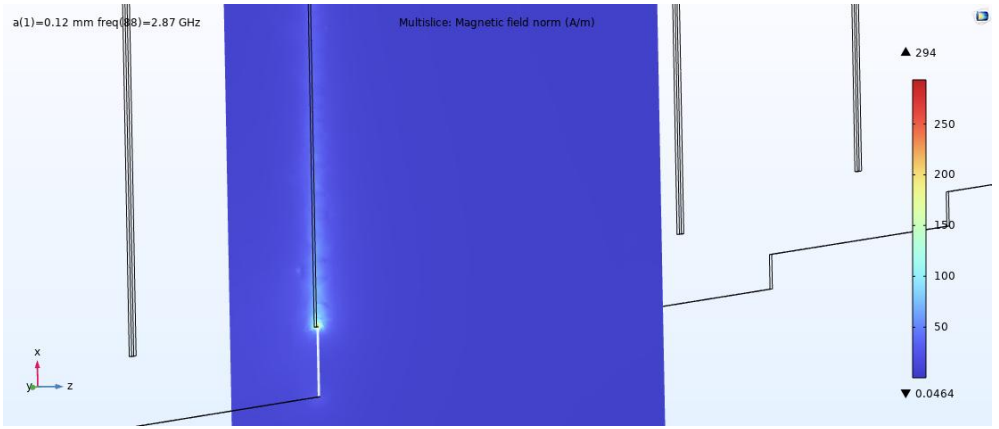

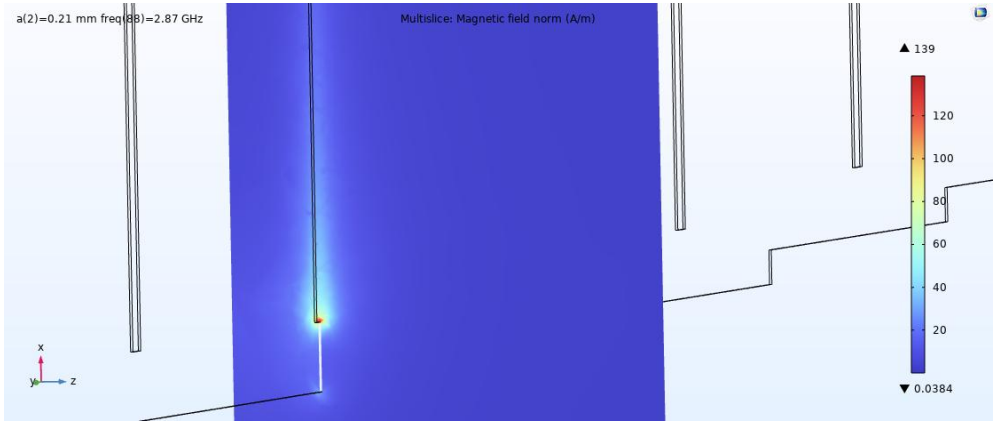

Simulations to measure magnetic field norm (zoomed in the gap).

Post-Fabrication Simulations

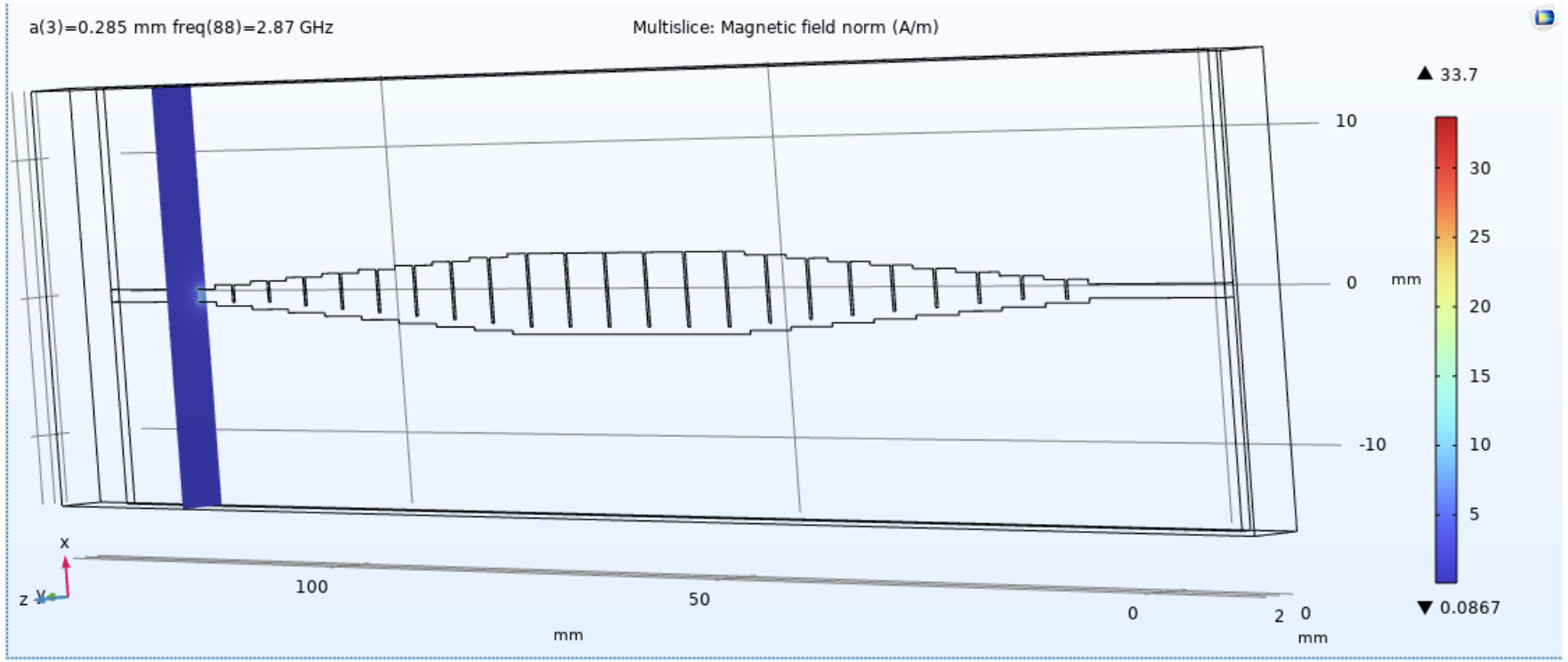

Simulation of the XZ-plane used to measure magnetic field norm on the microstrip (A/m).

Post-Fabrication Simulations

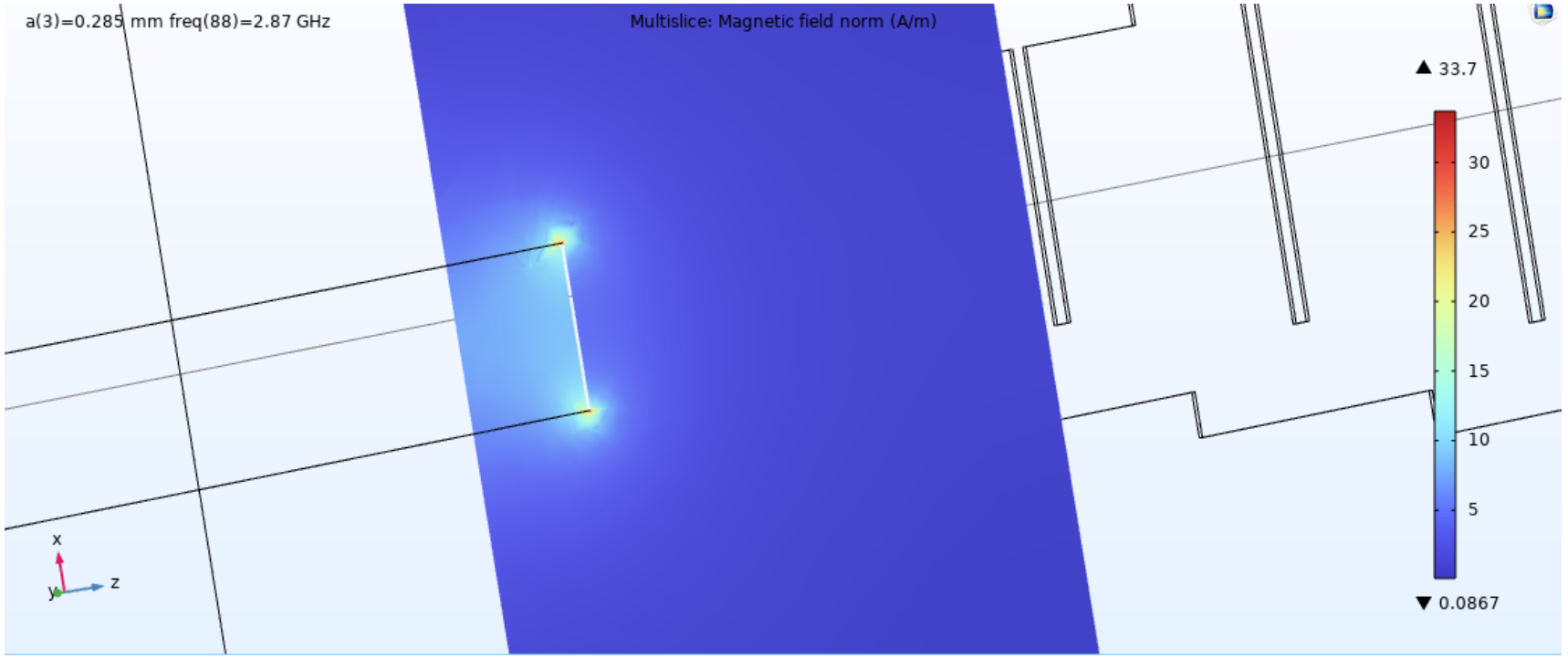

Simulations to measure magnetic field norm (zoomed in the microstrip region).

Gap Region ODMR Plot: Re-run

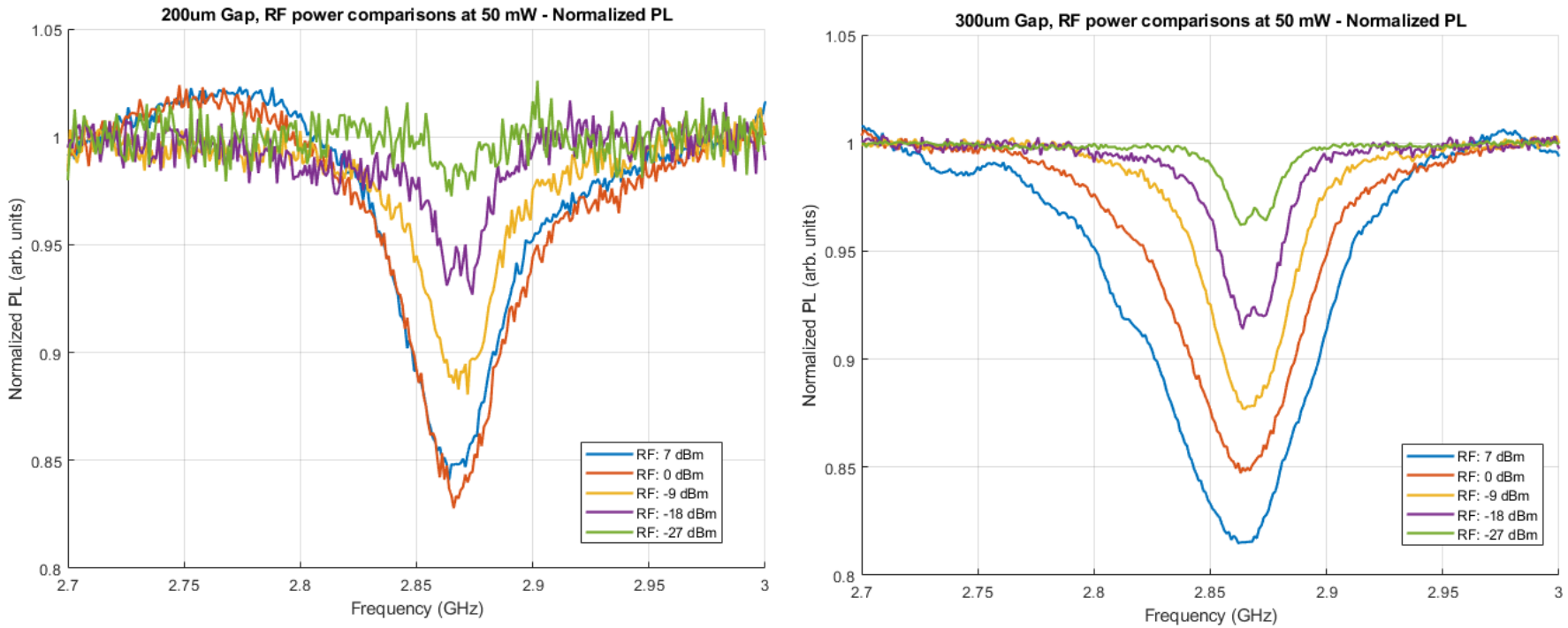

ODMR plots at varying RF power with the laser aligned towards the bottom of the gap.

Simulations: Magnetic Field Distribution

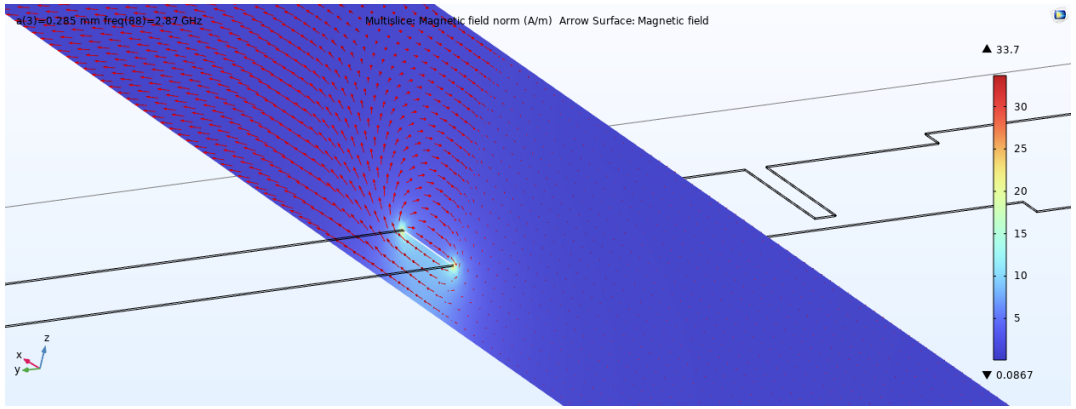

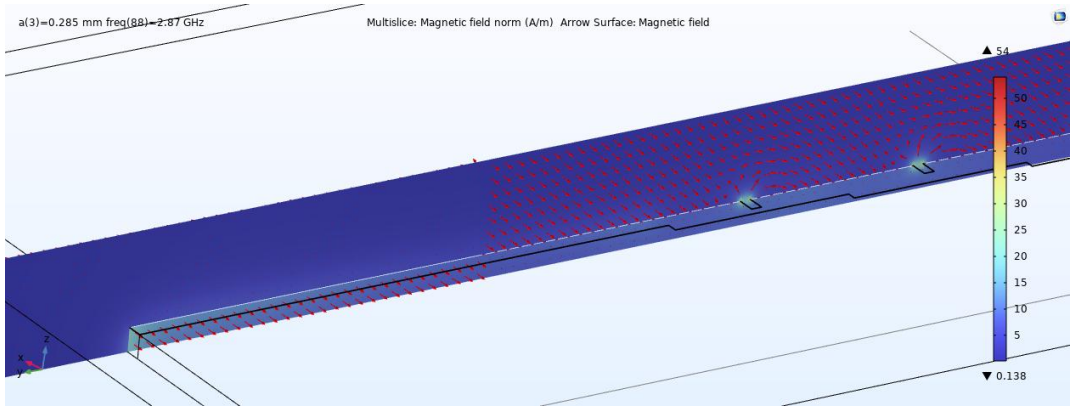

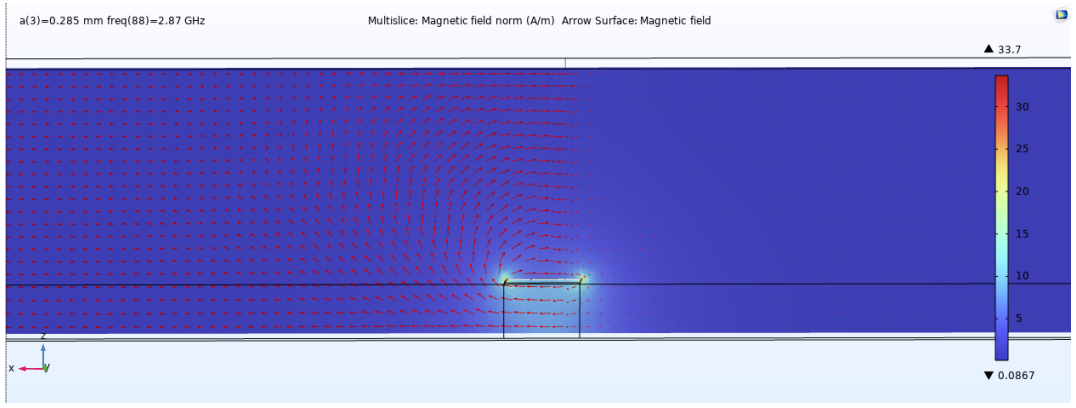

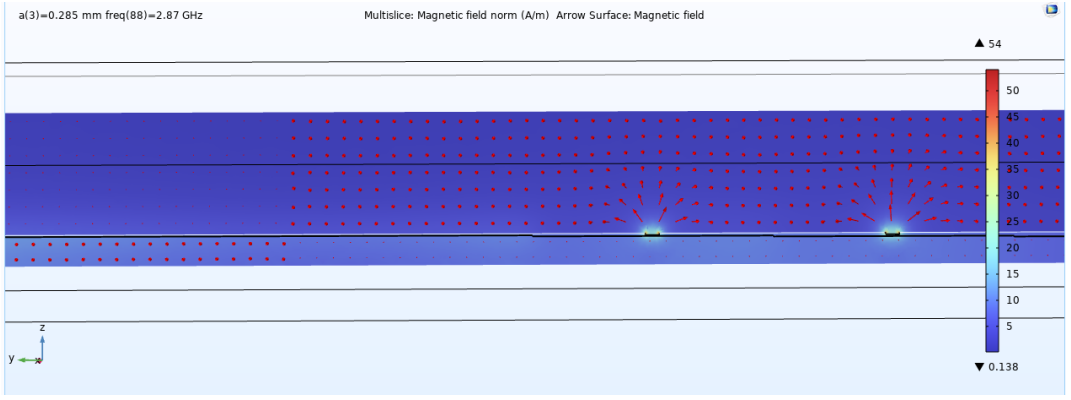

Simulation of the microstrip region and its corresponding magnetic field distribution (XZ and YZ planes).

Simulations: Magnetic Field Distribution

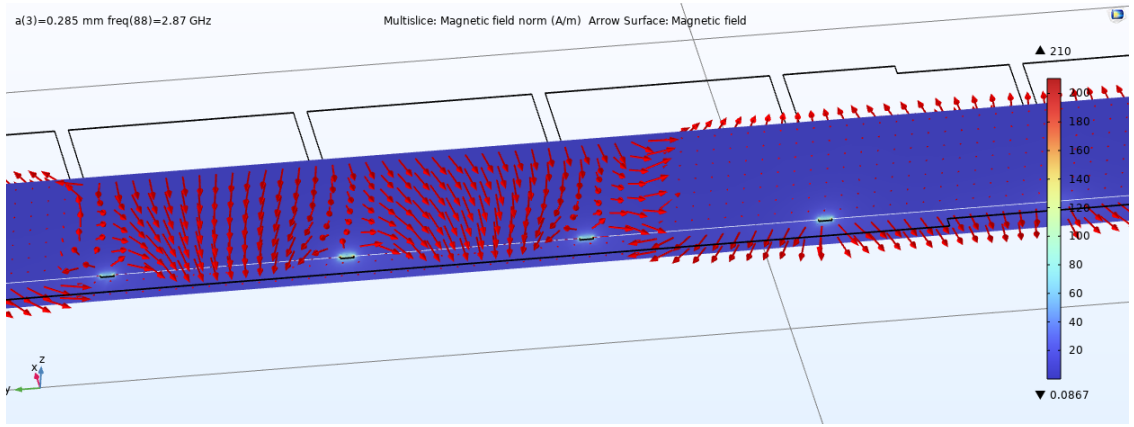

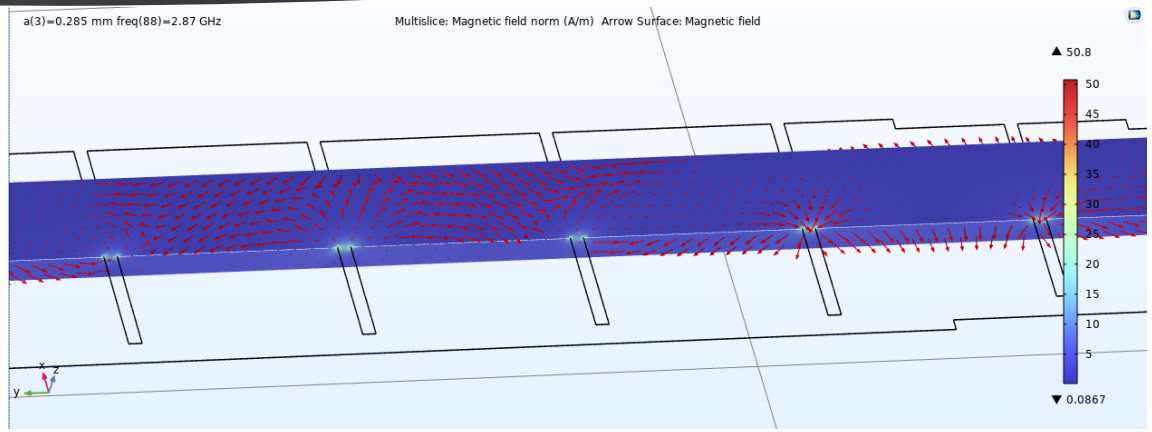

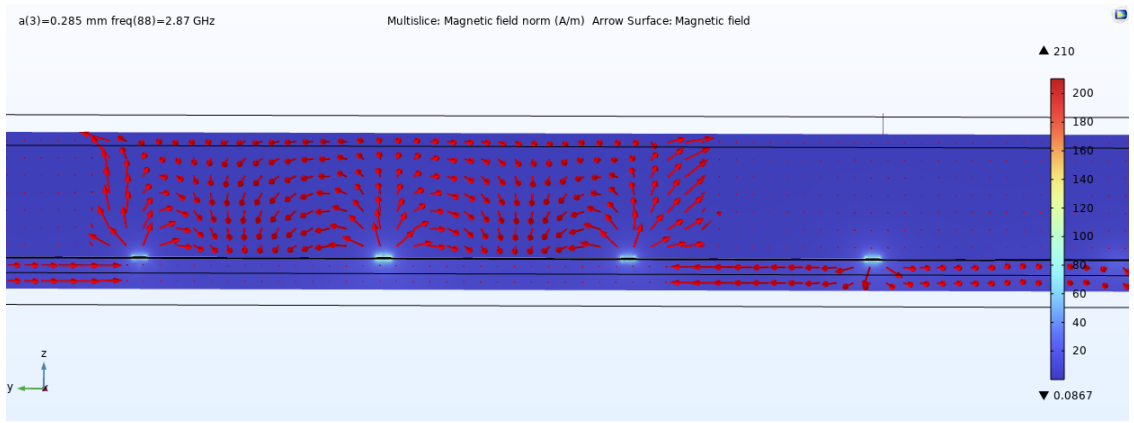

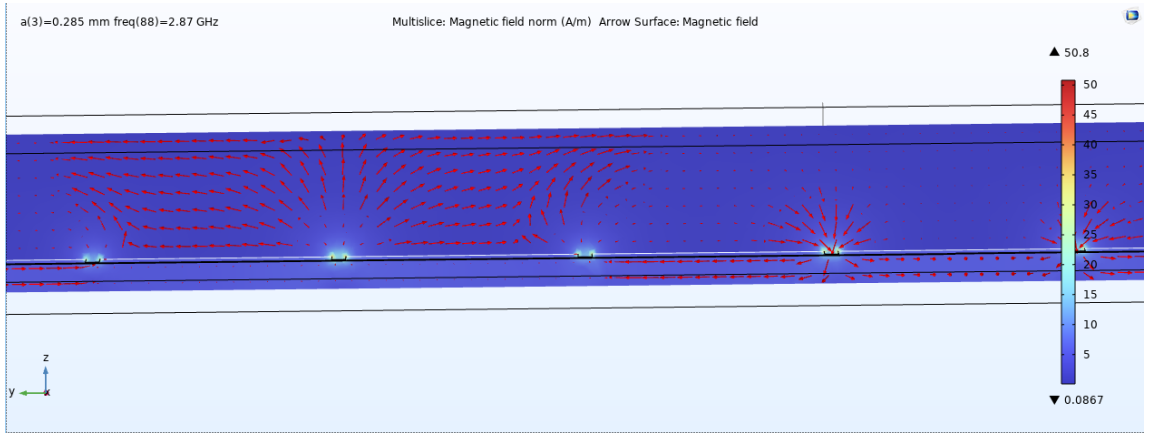

Simulation of the gap (near the bottom) and its corresponding magnetic field distribution (285μm version).

Simulations: S-Parameters

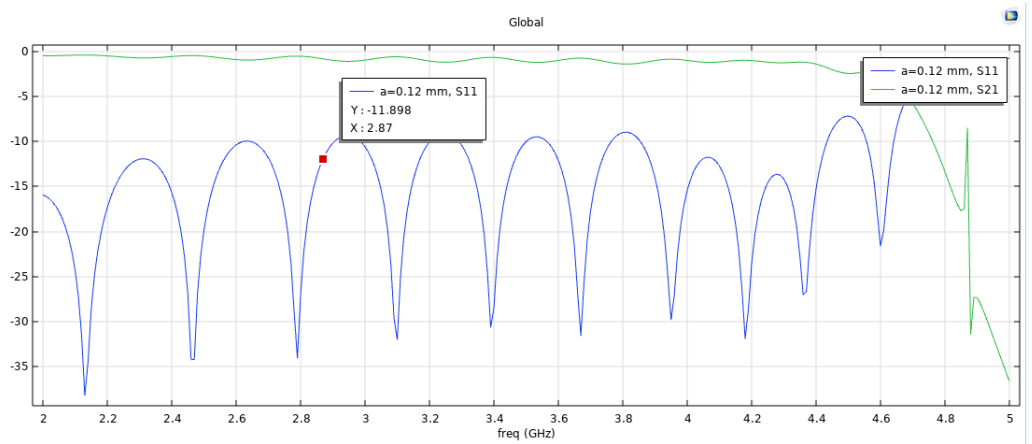

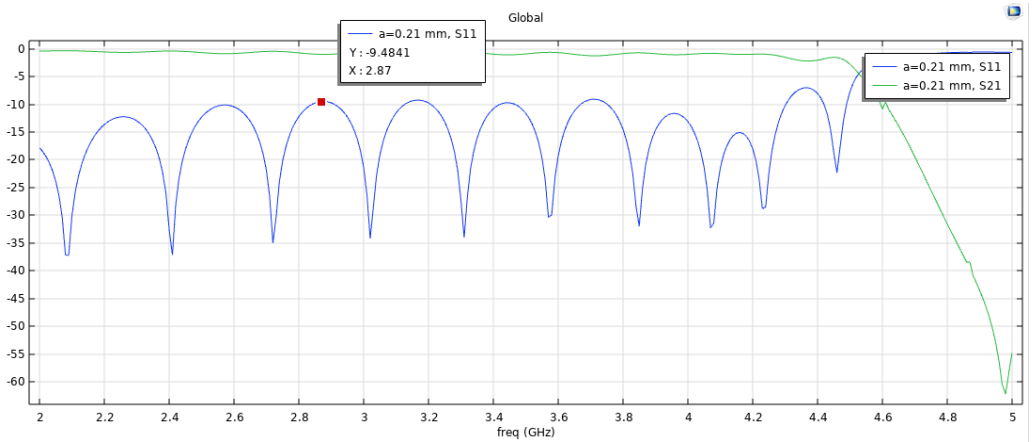

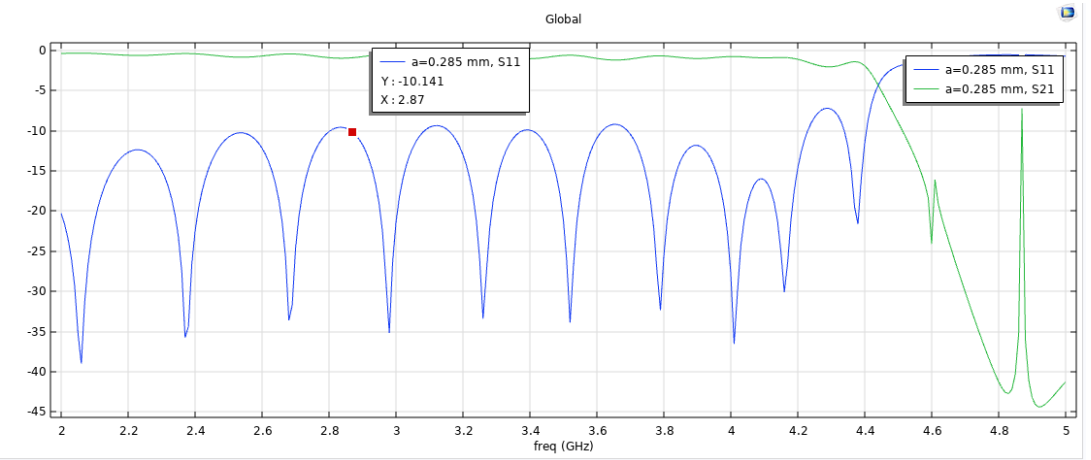

Simulated Waveguides: S11 and S21 plots of each waveguide variation

Simulations: S-Parameters

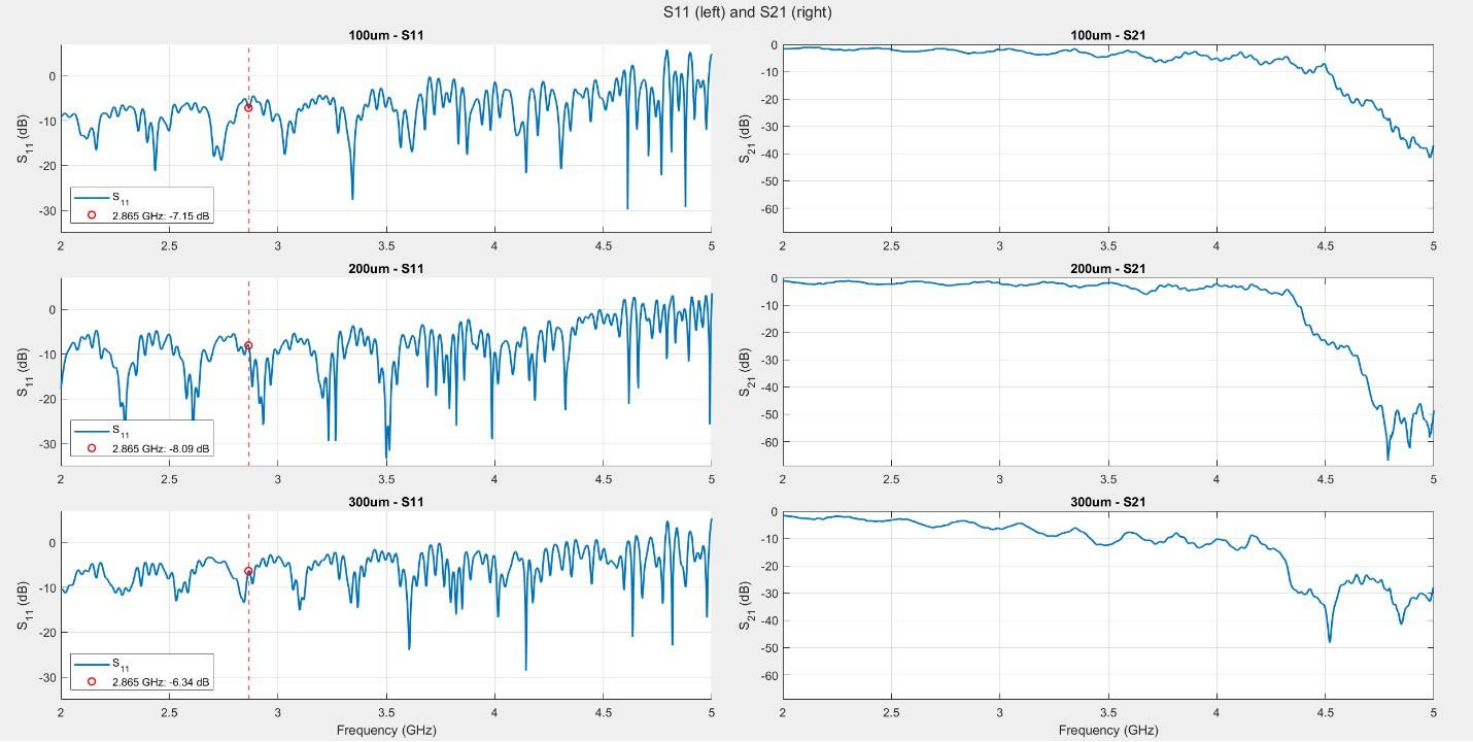

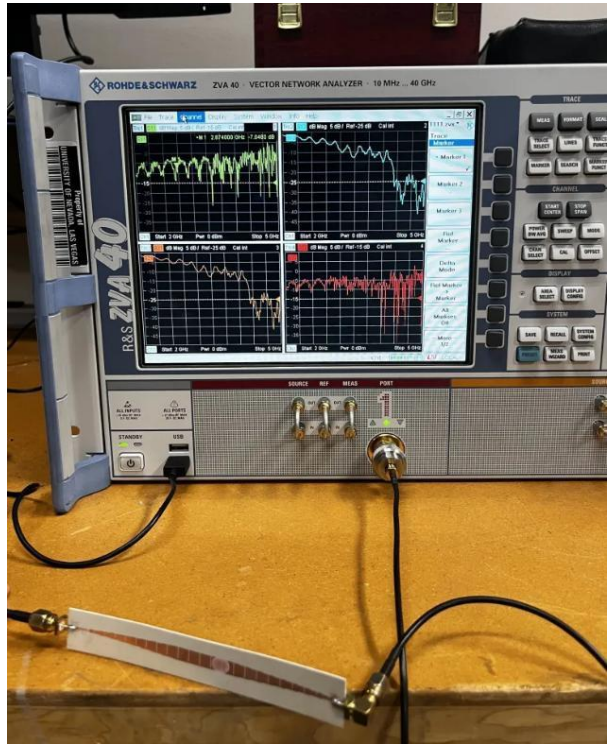

Fabricated Waveguides: S11 and S21 plots of each waveguide variation

Summary and Conclusion

- Characterized different gap sizes to compare field enhancement (experimental and simulated)
- NV center integration and ODMR characterization:
  - Magnetic field splitting
    - Confirmed consistent Zeeman splitting among repeated tests
  - Temperature shifting
    - Analyzed trends on how resonant frequencies shift (average slope of -175kHz/K)
    - Localized heating at the copper-dielectric interface is seen
  - Microwave power and optical power effects
    - Characterized how microwave power and laser intensities affect ODMR contrast, line-width and spin-driving efficiency

Conclusion and Future Works

- Characterize more dramatic gap differences (100μm vs 1mm)
- Resonant frequency shifts due to localized heating could affect gap size comparisons.
- Further reduce gap sizes down below 100μm
- Improve fabrication methods (stitching issues)
- Top-down setup for convenience (mainly thermal setup)
- Variation of objectives with longer working distances

Questions and Discussion